Available online at www.sciencedirect.com
SCIENCE DIRECT
Lithos 90 (2006) 19–42
LITHOS
www.elsevier.com/locate/lithos

Multistage metasomatism in ultrahigh-pressure mafic rocks from the North Dabie Complex (China)

Nadia Malaspina [a,*], Jörg Hermann [b], Marco Scambelluri [a], Roberto Compagnoni [c]

[a] Dip. per lo Studio del Territorio e delle sue Risorse, University of Genova, Corso Europa, 26, 16132 Genova, Italy
[b] Research School of Earth Sciences, Australian National University, Mills Road, 0200 Canberra, ACT, Australia
[c] Dip. di Scienze Mineralogiche e Petrologiche, University of Torino, Via Valperga Caluso, 35, 10125 Torino, Italy

Received 20 June 2005; accepted 3 January 2006
Available online 10 March 2006

Abstract

Release of metamorphic fluids within the slab and/or from the slab to the mantle wedge in subduction environments can produce important metasomatic effects. Ultrahigh-pressure (UHP) metasomatised rocks represent ideal materials to study the element exchange at pressures corresponding to sub-arc depths in subduction zones. We present a petrologic and geochemical study of eclogites (s.l.) from the Dabie Mountains (China). The investigated samples were collected in the North Dabie Complex, where eclogite-facies rocks are significantly overprinted by granulite-facies metamorphism and partial melting. The studied eclogites are included in meta-lherzolitic bodies, which are in turn hosted by leucocratic gneisses. The textural relations among the various rock-forming minerals enabled us to identify several re-crystallisation stages. The peak (UHP) paragenesis consists of garnet, clinopyroxene and rutile. UHP garnet and clinopyroxene display oriented inclusions of polycrystalline rods of rutile +ilmenite and of albite, K–Ba-feldspar and quartz, respectively. Garnet and clinopyroxene are both rimmed by an inclusion free zone that formed after the peak, still at high-pressure conditions. Such optical zoning does not correspond to a difference in major element concentrations between garnet core and rim. This observation provides evidence that the major element composition of garnet was reset during exhumation, thus preventing thermobarometric determination of peak metamorphic conditions. Further decompression is documented by the formation of limited ilmenite+amphibole and granulite-facies coronas consisting of clinopyroxene, orthopyroxene, plagioclase and amphibole around garnet. In order to investigate the stability of observed mineral parageneses, a series of reconnaissance piston cylinder synthesis experiments were carried out in an identical bulk composition. The experimental study indicates that the peak metamorphic paragenesis is stable at $P \sim 3.5$ GPa and $T \geq 750$–800 °C. The petrological study, combined with bulk-rock and mineral trace element analyses, provides evidence of intense metasomatism affecting these eclogites. The bulk-rock major and trace element compositions indicate that the eclogites derive from basaltic protoliths with MORB and E-MORB affinity. Compared with such basalts, the studied rocks show strong depletion in SiO_2 and alkalis and enrichment in MgO and FeO. These features likely derive from element exchange with ultramafic rocks prior to subduction, possibly related with the influx of Si-depleted and Mg-enriched fluids produced during the serpentinisation of the associated lherzolitic rocks. On the other hand, the trace element bulk-rock compositions show strong enrichment in Cs, Ba and Pb. The same characteristic enrichment and fractionation is recorded by peak metamorphic clinopyroxene but not in retrograde amphibole. Therefore, influx of crustal fluids transporting LILE and light elements must have occurred during subduction at UHP

* Corresponding author. Tel.: +39 0103538137; fax: +39 010352169.
E-mail address: malaspina@dipteris.unige.it (N. Malaspina).

0024-4937/$ - see front matter
doi:10.1016/j.lithos.2006.01.002

conditions. This stage likely records the tectonic coupling of the mafic–ultramafic rocks with the associated crustal rock units and provides evidence of LILE mobility between different slab components.

Keywords: Subduction; Trace element mobility; Ultrahigh-pressure fluids; Metasomatism; Mafic and ultramafic rocks; North Dabie Complex; China

1. Introduction

It is widely accepted that subduction zones are the channelways for element exchange between outer and inner shells of the Earth, leading to element recycling in the mantle and causing chemical differentiation of the Earth (Taylor and McLennan, 1985; Schmidt and Poli, 1998). These processes are largely fluid-mediated, since the release of metamorphic fluids by the subducting plate is accompanied by element mobility and transfer to the mantle wedge (Tatsumi et al., 1986; Brenan et al., 1995; Kogiso et al., 1997). Mobility of fluids within the slab and/or from the slab to the mantle wedge can produce important metasomatic effects. Unravelling processes of fluid-mediated element exchange between rocks that are characteristic of subducted crust and the mantle wedge is thus of primary importance in understanding element mobility in subduction zones. Several studies have addressed element transfer related to fluid release during prograde metamorphism in subduction zones (Bebout et al., 1999; Becker et al., 2000; Scambelluri and Philippot, 2001; Spandler et al., 2003). Nevertheless, detailed studies documenting interactions between felsic, mafic and ultramafic rocks at pressures corresponding to sub-arc depth in subduction zones are still scarce. For this reason, high-pressure (HP) and especially ultrahigh-pressure (UHP) metasomatised rocks are an ideal natural laboratory to study element exchange processes in a subduction zone environment.

A large number of workers have reported eclogitic and ultramafic rocks with relics of UHP metamorphism from the Central Dabie Shan (China) (Hacker et al., 1996; Liou et al., 1996; Zhang and Liou, 2000, 2003). By contrast, much less data are available from the northern part of the Dabie Shan, the North Dabie Complex, where the eclogite-facies rocks are overprinted by significant granulite-facies metamorphism and partial melting. At this location, evidence for UHP metamorphism has been reported by Tsai (1998) and Tsai et al. (2000), who described quartz segregations in clinopyroxene, as the result of decompression of a former supersilicic clinopyroxene. The processes governing the origin and evolution of these rocks, however, are still unknown and there are few constraints on UHP metamorphic conditions.

Here we present evidence of intense metasomatism affecting UHP rocks from the North Dabie Complex by means of a petrological and geochemical study. We propose that these rocks record repeated metasomatic exchanges with fluids characterised by different geochemical imprints. The aim of this work is (i) to characterise the geochemical composition of these rocks, (ii) to give constraints on their metamorphic evolution and (iii) to portray the major and trace element exchange that occurred from low to HP/UHP metamorphic conditions. We have tackled these problems following two integrated approaches: (i) a petrologic and geochemical study of natural rock samples and (ii) piston cylinder synthesis experiments using an identical bulk composition to the studied natural rocks. The results provide new constraints on the metamorphic evolution of the NDC and shed new light on element mobility in deeply subducted crustal rocks.

2. The North Dabie Complex: geological and petrological background

The Dabie orogenic belt has been divided into three main complexes on the basis of lithologic associations and of their metamorphic evolution (Liou et al., 1996; Hacker et al., 1998; Faure et al., 1999; Hirajima and Nakamura, 2003): 1) the southern Dabie, recording peak HP blueschist–greenschist facies metamorphism (Faure et al., 2003); 2) the central Dabie, with an HP to UHP overprint (Okay et al., 1989; Wang et al., 1989a,b; Wang and Liou, 1991; Xu et al., 1992; Cong et al., 1993; Zhang et al., 1995); and 3) the northern Dabie complex (NDC). The NDC predominantly consists of granitoids, orthogneisses, migmatites, metasediments with subordinated garnet-bearing amphibolites, eclogites, granulites and ultramafic rocks (Okay et al., 1993, Zhang et al., 1996, Jahn et al., 1999; Liu et al., 2005). Large volumes of the NDC underwent granulite- to amphibolite-facies metamorphism, accompanied by diffuse partial melting of felsic lithologies. Despite this pervasive high temperature overprint, three metamorphic stages were recognised in the NDC (Xu et al., 2000;

Liu et al., 2001; Xu et al., 2002): (1) an eclogite-facies stage, with $P=2.5$ GPa and $T=800–870$ °C, witnessed by the presence of eclogites, garnet-pyroxenites (Tsai and Liou, 1997; Tsai, 1998; Liu, 2000; Tsai and Liou, 2000) and by ultramafic rocks considered by Tsai et al. (2000) as retrogressed garnet-peridotites; (2) a retrograde HP granulite-facies stage, with $P=1.1–1.4$ GPa and $T=820–910$ °C; (3) a retrograde amphibolite-facies stage, with $P=0.5–0.6$ GPa and $T=500–600$ °C.

Recently, Tsai and Liou (2000) documented the occurrence of oriented quartz lamellae in clinopyroxene of some garnet-pyroxenites (eclogites s.l.), likely suggesting a former UHP stage. Geochemical and geochronological studies of several NDC eclogites and orthogneiss country rocks, indicate that the two rock types record a common metamorphic history during continental subduction in the Triassic (Liu et al., 2000; Xie et al., 2001; Liu et al., 2005). This being the case, it should be noted that no UHP minerals have been reported in the NDC orthogneisses so far and the geodynamic evolution of the complex is still debated (Hacker et al., 2000; Bryant et al., 2004).

3. Petrography

The investigated samples (RPC608, RPC609 and RPC610) are representative of the NDC rocks which underwent UHP metamorphism. They are three eclogites (s.l.) collected in the Shan Guan Tuan locality (Fig. 1). Despite the poor exposure, field relations indicate that the eclogites form layers included in ultramafic rocks, which show amphibolite-facies retrogression. The ultramafic body is in turn hosted by leucocratic gneisses. The structural relations among the different rock types are not well estabilished, and the relative timing of their coupling is not well constrained. Xu et al. (1994) and Tsai and Liou (1997) reported that the ultramafic rocks consist mainly of Cr-spinel harzburgite, dunite, and lherzolitic mylonite and are in tectonic contact with the hosting migmatitic orthogneisses. The ultramafic body is surrounded by minor plagioclase hornblendite dikes postdating the amphibolite-facies retrogression of lherzolites (Tsai, 1998).

The studied eclogite samples are slightly foliated and characterised by a porphyroblastic texture with millimetre-sized clinopyroxene and garnet (Fig. 2). The rock matrix consists of ilmenite, pargasitic hornblende, orthopyroxene + clinopyroxene + amphibole and amphibole + spinel + plagioclase symplectites, and accessory rutile and apatite. Quartz is neither present in the matrix parageneses nor as inclusion in garnet.

The textural relations among the various rock-forming minerals enabled us to identify several recrystallisation stages (Fig. 3). The oldest recognised paragenesis consists of clinopyroxene, garnet and rutile, which likely developed at UHP peak conditions.

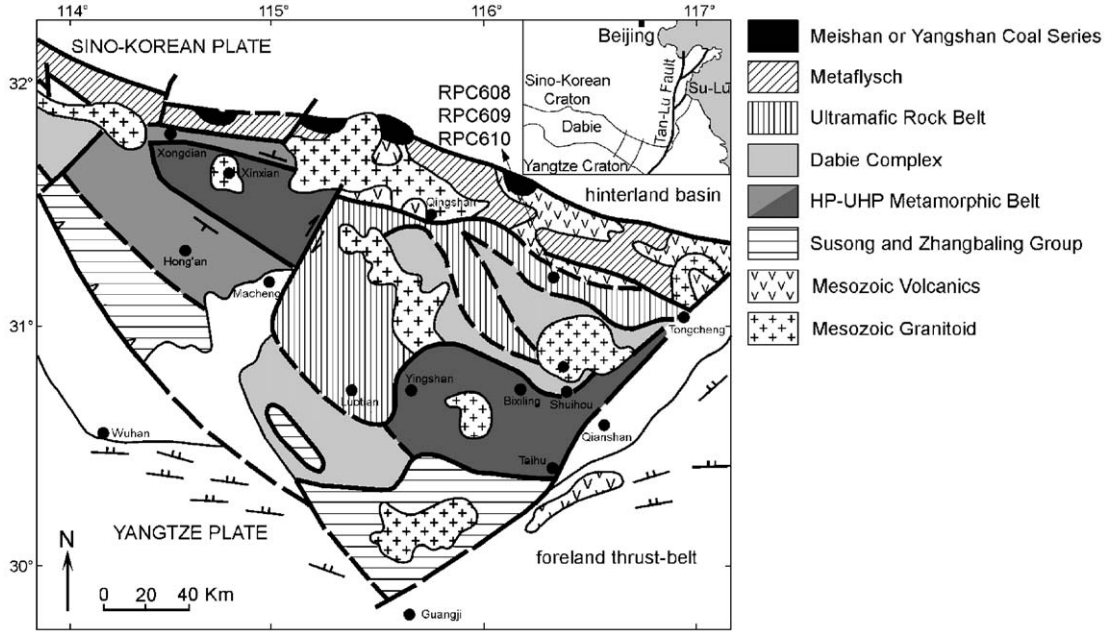

Fig. 1. Simplified tectono-metamorphic map of the Dabie Shan, with location of the UHP eclogite samples RPC608, RPC609 and RPC610, modified after Rolfo et al. (2004). Inset: geographic location of the Dabie belt in Eastern China.

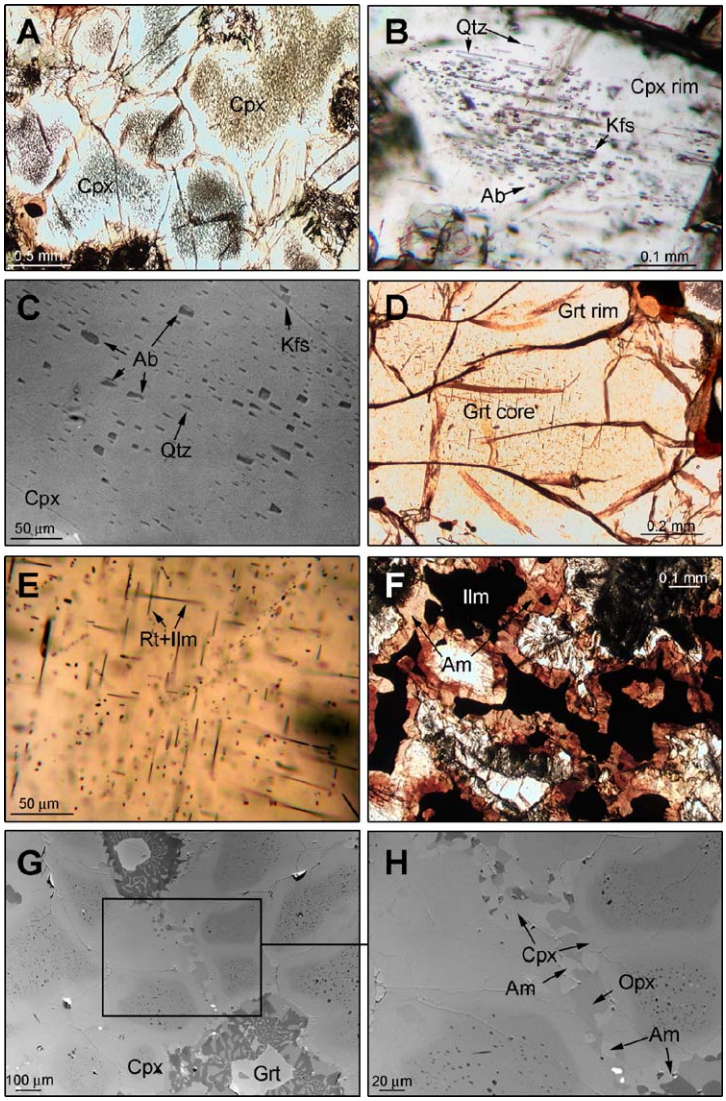

Fig. 2. Photomicrographs (transmitted light and BSE images) of representative rock-forming minerals and oriented lamellae from North Dabie Complex eclogites. A: Zoned clinopyroxene; cores with oriented needles and clear rims (plane-polarised light, PPL). B: Lamellae-rich domain in clinopyroxene (PPL). C: BSE image of oriented albite, quartz and K-feldspar lamellae in clinopyroxene core. D: Zoned garnet with core containing oriented rods of Ti-phases and clear rims. (PPL). E: Crystallographically oriented rutile+ilmenite rods in garnet core (PPL). F: Xenoblastic ilmenite grains rimmed by pargasitic amphibole (PPL). G: BSE image of zoned clinopyroxene and garnet partially replaced by a orthopyroxene+amphibole+spinel+plagioclase kelyphitic rim. H: Microvein filled with orthopyroxene, clinopyroxene and amphibole bridging kelyphites around garnets. Mineral abbreviations from Bucher and Frey (1994).

Porphyroblastic clinopyroxene is zoned and shows a dusty core displaying crystallographically oriented needles, and a clear inclusion-free rim (Fig. 2A and B). The mineral needles are 3–9 μm in diameter and about 10–50 μm in length. Back-scattered electron (BSE) microscopy images reveal that the oriented lamellae consist mainly of albite (~85 vol.%), quartz (~10 vol.%) and rare K-feldspar (~5 vol.%) (Fig. 2C). Under the optical microscope, quartz forms long and thin lamellae, whereas K-feldspar and albite lamellae are shorter and larger (Fig. 2B). Garnet appears zoned (Fig. 2D) and displays cores with abundant polycrystalline rods of rutile+ilmenite (3 μm in diameter and max 160 μm length), oriented according to three crystallographic directions (Fig. 2E). Larger idioblastic rutile crystals, locally occur in the garnet core. The garnet rim is clear and lacks rutile+ilmenite rods. Occasionally lamellae-free clinopyroxene and apatite are included in the garnet rim. This suggests that the crystallisation of albite+quartz+K-feldspar in clinopyroxene and of

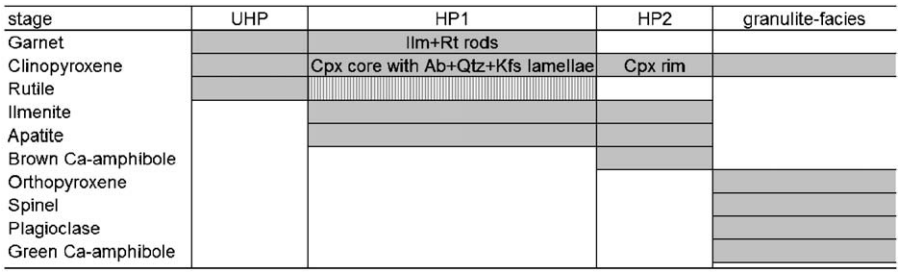

Fig. 3. Mineral parageneses at peak and retrograde metamorphic stages.

rutile+ilmenite in garnet occurred during decompression, at the transition from the UHP to HP_1 stage. At this stage (HP_1, Fig. 3) clinopyroxene and garnet coexist with apatite and ilmenite. Ilmenite is always included in brown pargasitic hornblende, which occurs as large xenoblastic crystals in the rock matrix, between clinopyroxene and garnet porphyroblasts (Fig. 2F; HP_2 in Fig. 3). Amphibole is stable with lamellae-free clinopyroxene rims developed at stage HP_2 (Fig. 3). The brown pargasitic hornblende is replaced by green amphibole+Al-green spinel symplectite. During this event, symplectites with green amphibole, orthopyroxene, plagioclase, ±green Al-rich spinel widely developed at the expense of porphyroblastic garnet (Fig. 2G). Symplectites are coarser in the outer portions around garnet and become progressively finer-grained towards the garnet relict (Fig. 2G). Microveins, filled with clinopyroxene, orthopyroxene and amphibole in textural equilibrium, bridge the retrograded garnet sites (Fig. 2H) and provide evidence for lower granulite-facies metamorphic conditions.

4. Analytical and experimental techniques

Bulk-rock major and trace elements were determined on rock glasses by standard XRF and Laser Ablation Inductively Coupled Plasma Mass Spectrometry (LA ICP-MS) at the Research School of Earth Sciences (RSES), The Australian National University (ANU, Canberra). To completely dissolve accessory minerals, the rock powders were fused with a flux of lithium tetraborate and lithium metaborate in the ratio 1:6.37 (0.2700 g sample and 1.7200 g flux) for major elements and in the ratio 1:3 (0.5 g sample and 1.5 g flux) for trace elements at 1200 °C for 20 min. Major elements were determined with a PW2400 wavelength-dispersive X-ray fluorescence (XRF) spectrometer housed at the Department of Earth and Marine Sciences (ANU). The FeO content of sample RPC609 was determined by standard wet-chemistry technique. Loss-on-ignition (LOI) was calculated as mass difference of 1 g of powdered sample after heating to 1000 °C for 1 h and correcting for weight gain due to ferrous iron oxidation. The LA ICP-MS technique employs an ArF (193 nm) EXCIMER coupled to an Agilent 7500 quadropole ICP-MS. A spot size of 187 μm was used and the counting time was 20 s for the background and between 40 and 45 s for sample analyses. ^{43}Ca and ^{29}Si were employed as the internal standard isotope, based on CaO and SiO_2 concentrations previously measured by XRF. NIST-612 glass was used as the external standard, assuming the composition given by Pearce et al. (1997). A BCR-2G glass was used as secondary standard. Reproducibility about the mean values of 6 analyses were between 0.5 and 4% relative (1σ) for the majority of elements. The average of this glass yielded trace element contents that were typically within 2–6% of the certified values for this standard (Wilson, 1997).

Major element of both eclogite minerals and experimental phases were analysed in energy dispersive mode with a Philips SEM 515 electron microscope at the University of Genova. The accelerating potential was 15 kV, the beam current 20 nA, and the counting time 100 s. Natural minerals were used as standard. Major elements were also determined by wavelength dispersive spectrometry using a Cameca SX 100 electron microprobe at the RSES, ANU. Acceleration voltage was set to 15 kV, beam current was 20 nA. Mineral analyses were always assisted by detailed back scattered electron (BSE) images to control the microtextural site.

Mineral trace elements were acquired by LA ICP-MS at the RSES (ANU), at similar running conditions as those described above, although spot sizes varied from 86 to 187 μm. All minerals were quantified using ^{29}Si as internal standard, except ^{49}Ti for ilmenite and ^{43}Ca for apatite.

A glass obtained from a powdered natural sample was used as starting material for the experimental study. We have selected RPC609 because it preserves best the UHP paragenesis. Fusion of the rock powder was obtained by passing a current of up to 8 Amps through a 0.3 mm thick molybdenum strips that was

placed in a sealed steel container. Five bars of argon pressure in the container prevented loss of volatile elements during melting and oxidation of iron. Rapid quenching was achieved by simultaneously turning off the current and dropping the argon pressure to 1 bar. Experiments were run in an end-loaded 1.27 cm piston-cylinder apparatus at the RSES (ANU). Fifteen to twenty milligrams of sample were loaded in a Au capsule (outside diameter=2.3 mm), and 5 wt.% of H_2O was added with a micro-syringe. The capsule was sealed by arc welding. The capsule was maintained below 100 °C during welding by immersion in water-soaked tissue paper. A low friction assembly was used consisting of teflon foil, NaCl and pyrex sleeves, a graphite heater and sintered MgO inserts, in which the Au capsule was embedded. The oxygen fugacity was not buffered, however the used assembly seems to buffer experiments close to Ni–NiO (W.O. Hibberson, pers. comm.). Pressure in the experiments was measured by load on the piston and is accurate to ±0.1 GPa. Pressure was adjusted several times during the first 24 h of runs to compensate for pressure drop caused by the release of internal friction. Temperature, controlled using type B thermocouples ($Pt_{94}Rh_6/Pt_{70}Rh_{30}$), was accurate to ±10 °C. At the end of the run, capsules were recovered, the sample exposed and mounted in epoxy.

5. Bulk-rock composition

5.1. Major elements

The major and trace element compositions of the investigated samples are reported in Table 1. Overall, the three analysed samples display mafic compositions, with Mg# ranging from 61 to 68, moderate Ni–Cr concentrations, and Al_2O_3 and CaO contents around 14–15 and 10–12 wt.%, respectively. Nevertheless, with respect to mafic rocks they show very low SiO_2 (43.6–45.7 wt.%), high MgO (11.7–15.3 wt.%) and $Fe_2O_{3_{tot}}$ (13.5–15 wt.%) contents. In order to constrain metasomatic changes, the major element compositions of samples RPC608, RPC609 and RPC610 are compared in Fig. 4 with the average composition of Mid Ocean Ridge Basalts (Normal-MORB from Hofmann, 1988; Transitional-MORB from Schilling et al., 1983), of Continental Tholeiitic Basalts (Lightfoot et al., 1990; Peng et al., 1998; Crocket and Paul, 2004), and spinel- and garnet-lherzolites (McDonough, 1991). Also reported are eclogites from the Raobazhai area of the NDC (data from Tsai and Liou, 2000), and eclogites from the northern Dabie Mountains collected in different localities (data from Liu et al., 2005). As a whole, the major element variability of both RPC608, RPC609, RPC610 and eclogites from Raobazhai are closely related to the composition of basaltic rocks, although their composition is displaced towards higher MgO contents. For a number of elements, the compositions of the studied eclogites plot on a mixing line between mafic and ultramafic rocks, generally falling close to the field of mafic rocks (Fig. 4).

Table 1
Bulk-rock major (wt.%) and trace (ppm) element compositions

Sample	RPC608	RPC609	RPC610
SiO_2	43.57	45.66	43.82
TiO_2	0.92	1.23	1.07
Al_2O_3	14.80	13.74	14.58
Fe_2O_3	14.4†	3.09	15.1†
FeO		10.44	
MgO	15.31	12.55	11.72
MnO	0.33	0.24	0.34
P_2O_5	0.03	0.08	0.31
CaO	9.89	12.14	11.35
Na_2O	0.69	1.65	1.49
K_2O	0.07	0.04	0.05
LOI	0.77	0.91	1.06
total	100.81	101.77	100.84
Mg#	68	65	61
Cu	26.8	16.8	119
Zn	15.1	23.9	30.3
Cr	945	529	378
Sc	62.7	53.0	55.5
Ni	138	199	110
Rb	1.84	1.37	1.51
Sr	388	432	487
Y	37.4	25.8	43.5
Zr	61.1	52.0	65.7
Nb	2.92	5.14	7.89
Cs	0.17	0.12	0.16
Ba	39.6	81.5	87.0
La	4.27	7.51	122
Ce	12.8	18.1	198
Pr	2.04	2.67	20.7
Nd	9.07	11.8	66.9
Sm	2.88	3.51	10.6
Eu	1.10	1.23	2.78
Gd	4.93	4.66	9.97
Tb	0.96	0.74	1.52
Dy	6.74	4.85	9.21
Ho	1.42	1.01	1.68
Er	4.14	2.93	4.47
Tm	0.59	0.42	0.60
Yb	3.87	2.91	3.79
Lu	0.59	0.43	0.54
Hf	1.80	1.62	1.92
Ta	0.20	0.28	0.57
Pb	14.5	7.87	10.2
Th	0.08	0.09	6.07
U	0.11	0.07	0.21

†=Total iron as Fe_2O_3. Mg#=Mg number.

5.2. Trace elements

The full dataset of trace elements analysed (Rare Earth Elements, REE; Large Ion Lithophile Elements, LILE; and High Field Strength Elements, HFSE) is reported in Table 1 and portrayed in Fig. 5. The Primitive Mantle normalised (×PM) REE compositions of the eclogite samples are shown in Fig. 5A. RPC608 and RPC609 display rather flat REE patterns with absolute concentrations at 10–15×PM. RPC609 is slightly richer in light REE (LREE) than RPC608, whereas RPC610 shows a LREE-enriched pattern (La=200×PM). In Fig. 5A the REE patterns of the three samples are compared with an average MORB (Hofmann, 1988) and with an average of tholeiitic basalts with continental affinity (CB) from the Deccan province (Lightfoot et al., 1990; Peng et al., 1998; Crocket and Paul, 2004). RPC608 and RPC609 patterns display a good overlap with MORB, likely suggesting that the protolith of these eclogites might have been basaltic in composition. RPC610 is richer in medium REE (MREE) and LREE contents with respect to the other two samples.

The full spectrum of analysed trace elements is shown in Fig. 5B and is compared with the reference MORB and CB. A progressive increase in U, Nb, Ta and LREE features the transition from RPC608 to RPC609 and RPC610 following a pattern approximately complementary to that of MORB. This progressive enrichment in incompatible elements indicates that RPC610 is the most differentiated of the studied samples (Wilson, 1989). This is supported by the Mg#, that decreases from 68 for RPC608 to 61 for RPC610 (Table 1). For the comparison with other basalt patterns we use the more primitive samples RPC608 and RPC609. As a whole, these two samples fit rather well with the MORB pattern for a large number of elements measured, particularly for the fluid-immobile elements like Nb, Ta, Zr, Hf, and Ti, (HFSE), heavy REE (HREE) and Sc. The most striking difference concerns the strong enrichment in fluid-mobile elements, with spikes of Cs, Ba, Pb, and Sr (LILE), and, to a minor extent, in LREE of the investigated samples with respect to MORB. A considerable difference with respect to MORB is

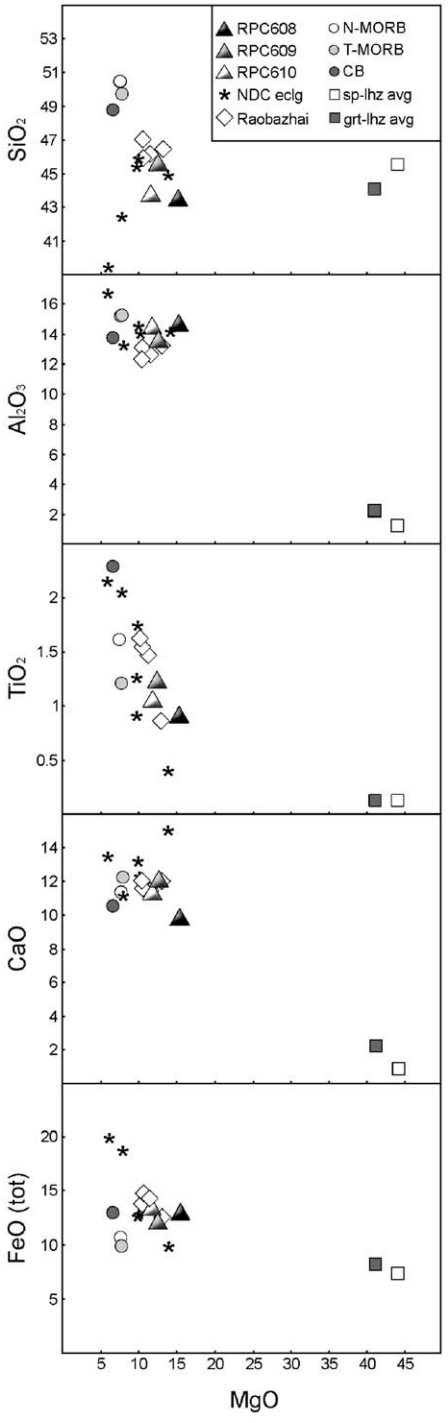

Fig. 4. Bulk-rock major element compositions of RPC608, RPC609 and RPC 610 (data from Table 1) compared with (i) average Normal-MORB (Hofmann, 1988), Transitional-MORB from Mid-Atlantic Ridge 34–38°N (Schilling et al., 1983) and average Continental Tholeiitic Basalts from Deccan province (Peng et al., 1998; Lightfoot et al., 1990; Crocket and Paul, 2004); (ii) average spinel- and garnet-lherzolites (Mc Donough, 1991); (iii) eclogites from Raobazhai, NDC (Tsai and Liou, 2000); (iv) eclogites from Huangweihe, Raobazhai, Baizhangyan, and Huazhuang, NDC (Liu et al., 2005). Abbreviations: sp-lhz=spinel-lherzolite, grt-lhz=garnet-lherzolite, NDC eclg=eclogites from Northern Dabie Mountains, avg=average.

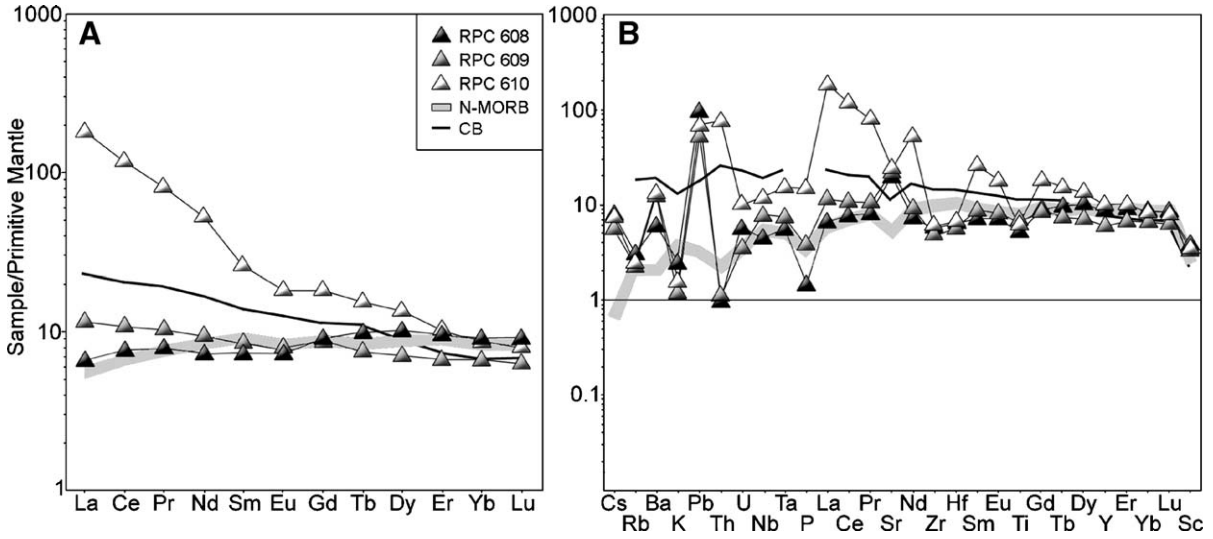

Fig. 5. Primitive mantle normalised REE (A) and other trace element (B) concentrations of RPC608, RPC609 and RPC610 (data from Table 1). Shaded grey area represents average N-MORB pattern (Hofmann, 1988); the black solid line is the average pattern of continental tholeiitic basalts from Deccan province (Lightfoot et al., 1990; Peng et al., 1998; Crocket and Paul, 2004). Normalising values after McDonough and Sun (1995). Elements are presented in order of increasing compatibility (left to right) during melting in the upper mantle (Hofmann, 1988; Sun and McDonough, 1989). Abbreviations: CB=continental tholeiitic basalts.

represented by lower Th/U ratio and a strong positive Sr anomaly in samples RPC608 and RPC609.

6. Mineral composition

6.1. Major elements

The major element compositions of the main rock-forming minerals are listed in Table 2. Clinopyroxene mostly corresponds to diopside and augite (Morimoto, 1989). Its composition shows a sharp zonation, as portrayed in Fig. 6, characterised by the progressive core-to-rim increase in FeO_{tot} and MgO, and by the complementary decrease in Al_2O_3 and Na_2O. The increase in FeO is visible as increasing brightness of the clinopyroxene in the BSE images (Fig. 2G and H). The change in composition coincides with the change from lamellae bearing to inclusion-free clinopyroxene domains. Interestingly, lamellae-free clinopyroxene which is included in garnet is unzoned in composition and displays the high Na_2O and low FeO contents that characterise the core composition of the large grains. Clinopyroxene in the recrystallised microveins displays the same composition as the outermost rims of the large grains.

The garnet composition corresponds to pyrope (~44 mol.%), almandine (~36 mol.%) and grossular (~20 mol.%). The FeO_{tot}, MgO and CaO concentrations in garnet do not show any important core-to-rim variation, except for a very thin outermost rim (Fig. 6). In this rim we observe an increase in FeO and a decrease in MgO which are likely related to retrograde equilibration. Additionally, the rims occasionally display much higher MnO contents than the core (Table 2), which we interpret to be related to limited garnet resorption. The most interesting feature in these garnet profiles is the lack of correlation between the major element composition and the observed optical zoning (Fig. 6), marked by the Ti-phases needles in the core (Fig. 2D). TiO_2 is the only minor element showing a compositional change in correspondence of the optical zoning (c.f. Figs. 2D and 6), decreasing from core (0.1 wt.%) to the exsolution-free rim (0.03 wt.%) (Fig. 6).

Both brown amphibole around ilmenite and the green amphibole in kelyphite are calcic. The brown amphibole composition varies from kaersutite, to tschermakitic hornblende, to pargasite, mainly as a consequence of the variation of TiO_2 and $(Na+K)_A$ (Leake et al., 1997). The green amphibole is a pargasite with low TiO_2 (less than 0.5 wt.%) and high FeO_{tot} (Table 2). Orthopyroxene, forming with spinel and plagioclase symplectites around garnet, is a bronzite and contains ~4 wt.% of Al_2O_3 (Table 2). Spinel is Al_2O_3-rich and the plagioclase is anorthite.

Due to the very fine grain size, oriented rods in clinopyroxene and garnet were mostly distinguished qualitatively by means of the scanning electron

Table 2
Major element compositions (wt.%) and structural formulae of representative peak and retrograde phases

Sample	RPC609					RPC610				RPC609				RPC610				RPC609						RPC608	
Mineral	Cpx core	Cpx core	Cpx rim	Cpx rim	Cpx∗	Cpx core	Cpx core	Cpx rim	Cpx rim	Grt core	Grt core	Grt rim	Grt rim	Grt core	Grt core	Grt rim	Grt rim	Am	Am	Ilm	Am kel	Cpx kel	Spl kel	Opx kel	Pl kel
SiO_2	53.63	54.13	52.30	52.44	54.65	54.40	54.32	51.62	51.34	41.12	40.81	41.00	40.30	41.42	41.20	41.03	40.84	40.39	40.18	0.04	41.75	51.69	0.25	52.12	44.01
TiO_2	0.06	0.06	0.22	0.16	0.05	0.08	0.08	0.06	0.04	0.11	0.10	0.02	0.04	0.09	0.10	0.04	0.04	3.09	5.38	52.79	0.35	0.20	0.27	0.15	0.15
Al_2O_3	3.70	3.57	2.87	3.07	3.16	4.74	4.74	3.83	3.59	23.07	22.98	23.01	22.99	22.39	22.31	22.09	22.08	14.42	15.93	0.02	16.35	2.82	59.82	3.98	35.90
Cr_2O_3	0.07	0.08	0.30	0.26	0.09	0.05	0.04	0.05	0.05	Bdl	0.01	0.02	0.03	0.02	0.01	0.03	0.03	0.06	0.15	0.04	0.29	0.34	0.29	0.11	0.29
FeO_{tot}	5.49	5.08	8.90	7.40	5.42	5.84	5.86	8.89	9.65	17.88	18.12	18.01	20.09	17.70	16.95	18.48	20.63	11.03	6.92	37.86	11.85	7.47	26.39	16.66	0.78
MgO	13.96	13.76	15.62	14.99	13.85	13.12	13.14	15.61	15.94	12.24	12.23	12.45	11.15	12.79	13.54	12.31	12.01	13.17	13.57	6.29	13.93	14.45	12.35	26.52	0.00
MnO	0.02	0.01	0.36	0.24	0.08	0.02	0.02	0.17	0.18	0.29	0.29	0.27	0.32	0.59	0.49	0.42	1.03	0.07	0.02	0.12	0.32	0.35	0.35	0.77	0.14
CaO	20.03	19.80	19.19	20.49	19.67	19.06	19.07	18.97	18.12	7.97	7.90	7.99	7.19	7.58	7.10	7.58	4.30	11.70	11.78	0.00	11.38	22.20	0.38	0.44	18.56
Na_2O	2.28	2.77	0.45	0.51	2.81	2.91	2.94	0.68	0.51	0.03	0.02	0.02	Bdl	0.03	0.04	Bdl	Bdl	3.37	3.62	0.01	2.79	0.11	Bdl	Bdl	0.36
K_2O	Bdl	Bdl	Bdl	Bdl	Bdl	Bdl	Bdl	Bdl	Bdl	Bdl	Bdl	Bdl	Bdl	Bdl	Bdl	Bdl	Bdl	Bdl	Bdl	Bdl	0.14	Bdl	Bdl	Bdl	0.21
Total	99.24	99.25	100.21	99.56	99.78	100.22	100.22	99.90	99.43	102.71	102.46	102.78	102.11	102.61	101.74	101.97	100.96	97.30	97.56	97.18	99.15	99.63	100.10	100.75	100.40
Si	1.96	1.97	1.93	1.94	1.98	1.97	1.96	1.90	1.90	2.98	2.96	2.97	2.96	3.00	3.00	3.00	3.04	5.93	5.79	0.00	5.99	1.92	0.01	1.86	2.03
Ti	0.00	0.00	0.01	0.00	0.00	0.00	0.00	0.00	0.00	0.01	0.01	0.00	0.00	0.00	0.01	0.00	0.00	0.34	0.58	0.98	0.04	0.01	0.01	0.00	0.01
Al	0.16	0.15	0.12	0.13	0.14	0.20	0.20	0.17	0.16	1.97	1.97	1.96	1.99	1.91	1.91	1.90	1.94	2.50	2.71	0.00	2.76	0.12	1.88	0.17	1.95
Cr	0.00	0.00	0.01	0.01	0.00	0.00	0.00	0.00	0.00	0.00	0.00	0.00	0.00	0.00	0.00	0.00	0.00	0.01	0.02	0.00	0.03	0.01	0.01	0.00	0.01
Fe^{2+}	0.09	0.06	0.24	0.21	0.07	0.11	0.11	0.19	0.22	1.02	1.01	0.98	1.16	0.99	0.94	1.04	1.30	1.355†	0.834†	0.782†	1.421†	0.19	0.589†	0.40	0.030†
Fe^{3+}	0.08	0.09	0.04	0.02	0.09	0.06	0.07	0.08	0.08	0.07	0.09	0.11	0.08	0.08	0.09	0.09	0.01					0.04		0.10	
Mg	0.76	0.75	0.86	0.83	0.75	0.71	0.71	0.86	0.88	1.32	1.32	1.34	1.22	1.38	1.47	1.34	1.30	2.88	2.91	0.23	2.98	0.80	0.49	1.41	0.00
Mn	0.00	0.00	0.01	0.01	0.00	0.00	0.00	0.01	0.01	0.02	0.02	0.02	0.02	0.04	0.03	0.03	0.06	0.01	0.00	0.00	0.04	0.01	0.01	0.02	0.01
Ca	0.78	0.77	0.76	0.81	0.76	0.74	0.74	0.75	0.72	0.62	0.61	0.62	0.57	0.59	0.55	0.59	0.34	1.84	1.82	0.00	1.75	0.88	0.01	0.02	0.92
Na	0.16	0.20	0.03	0.04	0.20	0.20	0.21	0.05	0.04	0.00	0.00	0.00	Bdl	0.00	0.01	Bdl	Bdl	0.96	1.01	0.00	0.78	0.01	Bdl	Bdl	0.03
K	Bdl	Bdl	Bdl	Bdl	Bdl	Bdl	Bdl	Bdl	Bdl	Bdl	Bdl	Bdl	Bdl	Bdl	Bdl	Bdl	Bdl	Bdl	Bdl	Bdl	0.03	Bdl	Bdl	Bdl	0.01
Cation sum	4.00	4.00	4.00	4.00	5.00	4.00	4.00	4.00	4.00	8.00	8.00	8.00	8.00	8.00	8.00	8.00	8.00	15.82	15.69	2.00	15.83	4.00	3.00	4.00	5.00

Clino- and orthopyroxenes are normalised on the basis of 4 cations and 6 oxygens. Garnet is normalised on the basis of 8 cations and 12 oxygens. Calcic amphibole is normalised on the basis of 23 oxygens. Fe^{3+} for clinopyroxene and garnet is calculated assuming stoichiometry (Droop, 1987). ∗=refers to lamellae-free clinopyroxene included in garnet rims; †=total iron as Fe^{2+}. Mineral abbreviations from Bucher and Frey (1994). Bdl=below detection limits, kel=kelyphite.

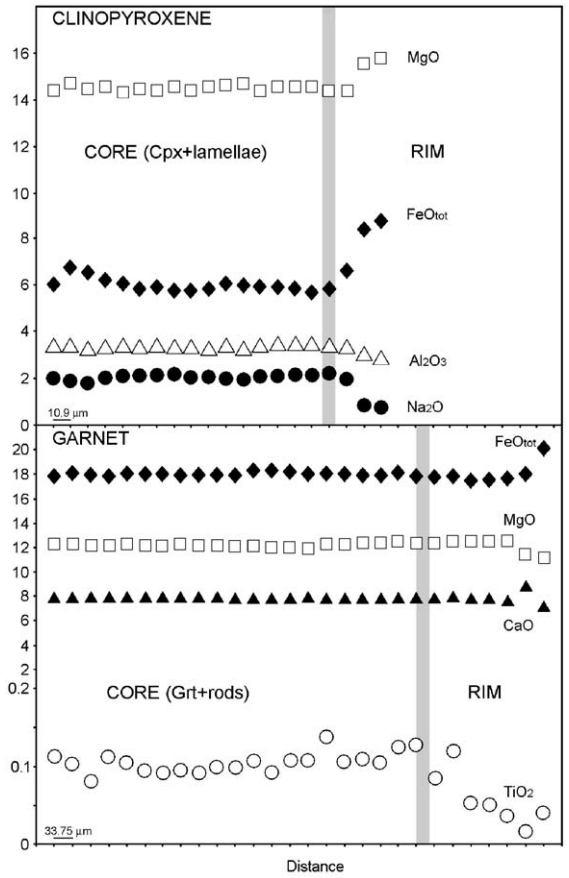

Fig. 6. Compositional variations along microprobe profiles in porphyroblastic clinopyroxene and garnet. The shaded line marks the core-to-rim boundary, as observed under the optical microscope and BSE images (Fig. 2A, D, G and H). The scale bar indicates the distance of point analyses.

microscope (SEM). The analysable lamellae in clinopyroxene are mostly albite and K-feldspar, the latter ranging in composition from K-feldspar to Ba–K-feldspar (0.14–0.32 BaO wt.%). Some representative analyses of albite, K-feldspar and ilmenite rods are reported in Table 3, together with the primary inferred clinopyroxene composition (Cpx+lam). The major element concentrations have been measured by integrating the lamellae with the clinopyroxene core composition, by means of electron microscope area analyses (windows 30 μm^2). Integration of albite and quartz lamellae leads to an original clinopyroxene composition that is characterised by higher SiO_2, Al_2O_3 and Na_2O contents, compared to the measured core composition. On the other hand, MgO and CaO are lower and the SiO_2/CaO ratio is higher than in lamellae-free clinopyroxene. Some garnets have also been analysed in this way to integrate the Ti-phase needles. The resulting TiO_2 content is only slightly higher and reaches 0.16 wt.%.

6.2. Trace elements

The trace element compositions of the UHP and HP minerals are listed in Table 4. They provide important information on the evolution and coexistence of the key minerals. Fig. 7 shows the REE and trace element patterns of representative UHP and HP mineral analyses, normalised to the Primitive Mantle. Garnet and clinopyroxene cores are characterised by absolute REE concentrations up to 20–30×PM (Fig. 7A): their patterns display a partitioning of LREE and HREE between the two minerals, indicating the attainment of a chemical equilibrium during their growth. Garnet is almost homogeneous in composition and no significant difference can be observed between core and rim. Garnet shows a strong fractionation with enrichment in HREE and depletion in LREE concentrations. Analyses in garnet cores include rods of rutile and ilmenite and consequently the Ti content of the core (from 390 to 670 ppm) is higher than the rim (250–230 ppm). Clinopyroxene has high LREE and generally low HREE abundances. It displays a core-to-rim zonation with progressive enrichment in HREE. This is in agreement with the microstructural observations, indicating a two-stage clinopyroxene growth: lamellae-rich cores grew in equilibrium with garnet, and rims formed during the progressive equilibration with post-peak minerals when garnet was no longer stable (Fig. 3). Fig. 7B reports the full spectrum of the analysed trace elements. Both garnet and clinopyroxene display large variation in the concentration of many trace elements, such as Ba, K, Pb, Nb, Sr. It is important to note that the Laser Ablation analyses were performed with a spot size varying from 86 to 187 µm. Therefore, the trace element composition of core domains both in garnet and clinopyroxene include also the contribution of rods and lamellae. Overall their trace element patterns display similar features as the bulk-rock (Figs. 5B and 7B). Clinopyroxene is characterised by a strong fractionation in LILE, with enrichment of Cs, Ba and Pb relative to Rb and K. Very high Ba concentrations can be present in clinopyroxene, which shows spikes up to 50×PM values. Garnet is characterised by highly variable Sr and generally high contents in HFSE.

The REE patterns of post-peak apatite, amphibole and ilmenite are reported in Fig. 7C. Apatite is characterised by a strong enrichment in LREE and MREE relative to depletion in HREE. Amphibole shows

Table 3
Major element compositions (wt.%) and structural formulae of analysable oriented rods in clinopyroxene and garnet

Sample	RPC609	RPC610			RPC609		Cpx+lam	Cpx core
Host mineral	Cpx				Grt			
Lamellae	Kfs	Kfs	Kfs	Ab	Ilm	Ilm		
SiO_2	64.93	65.67	64.22	67.56	0.07	Bdl	57.17	55.20
TiO_2	Bdl	0.05	Bdl	0.12	52.10	53.01	0.12	0.08
Al_2O_3	18.10	18.00	18.50	21.15	Bdl	Bdl	5.24	4.48
Cr_2O_3	Bdl	0.13	0.10	0.12	0.25	0.27	0.11	0.08
FeO_{tot}	0.46	0.36	0.49	0.34	37.86	39.38	5.08	5.74
MgO	Bdl	Bdl	Bdl	Bdl	6.81	5.25	12.21	13.37
MnO	Bdl	0.17	0.11	0.11	0.34	0.40	0.04	0.05
NiO	Bdl	0.08	0.12	0.15	0.39	0.44	Bdl	Bdl
CaO	0.34	0.37	0.46	0.54	0.55	0.25	17.05	18.71
Na_2O	Bdl	Bdl	Bdl	11.00	Bdl	Bdl	3.28	2.50
K_2O	16.30	15.51	15.96	0.09	Bdl	Bdl	0.02	Bdl
BaO	Bdl	0.14	0.32	Bdl	Bdl	Bdl	Bdl	Bdl
Total	100.13	100.48	100.28	101.18	98.37	99.00	100.32	100.21
Si	3.01	3.05	2.98	2.93	0.00	Bdl	2.04	2.00
Ti	Bdl	0.00	Bdl	0.00	0.95	0.97	0.00	0.00
Al	0.99	0.98	1.01	1.08	Bdl	Bdl	0.22	0.19
Cr	Bdl	0.00	0.00	0.00	0.00	0.01	0.00	0.00
Fe_{tot}	0.02	0.01	0.02	0.01	0.77	0.81	0.15	0.17
Mg	Bdl	Bdl	Bdl	Bdl	0.25	0.19	0.65	0.72
Mn	Bdl	0.01	0.00	0.00	0.01	0.01	0.00	0.00
Ni	Bdl	0.00	0.00	0.01	0.01	0.01	Bdl	Bdl
Ca	0.02	0.02	0.02	0.03	0.01	0.01	0.65	0.73
Na	Bdl	Bdl	Bdl	0.93	Bdl	Bdl	0.23	0.18
K	0.96	0.92	0.95	0.00	Bdl	Bdl	0.00	Bdl
Ba	Bdl	0.00	0.01	Bdl	Bdl	Bdl	Bdl	Bdl
Cation sum	5.00	5.00	5.00	5.00	2.00	2.00	3.96	3.99

K-feldspar and albite normalised on the basis of 5 cations and 8 oxygens. Ilmenite normalised on the basis of 2 cations. Average clinopyroxene+lamellae and clinopyroxene core without lamellae are both normalised on the basis of 6 oxygens. Lam=lamellae.

flat REE patterns, with HREE abundances comparable to that of clinopyroxene rims. This supports the textural observation, that amphibole is not in equilibrium with garnet. Ilmenite has very low LREE and MREE concentrations relative to HREE. Apatite and amphibole have low K and Ba normalised contents, even lower than clinopyroxene (Fig. 7D). Apatite shows very high Pb, Th, U and Sr concentrations, whereas it is strongly depleted in HFSE with low Nb/Ta and Zr/Hf ratios. On the other hand, HFSE are partitioned into ilmenite that shows very high Nb and Ta contents (Table 4).

7. Experimental results

7.1. Experimental strategy

To date, no experimental work has been reported in systems with a composition approaching that of the NDC samples reported here. Experiments in mafic systems are normally SiO_2-saturated at UHP conditions, whereas there is no evidence for stable quartz or coesite throughout the metamorphic evolution of the NDC eclogites (Fig. 3). To investigate the stability and composition of different phases and to better constrain peak metamorphic conditions, we performed a series of reconnaissance synthesis experiments that cover the possible P–T conditions encountered by the investigated eclogites. To facilitate the comparison between experiments and natural rocks, the employed experimental starting material had an identical composition to that of the natural samples. To achieve this, we produced a homogeneous glass from rock powders of sample RPC609. As the peak metamorphic paragenesis likely derived from a previous hydrous assemblage 5 wt.% of H_2O was added to all experiments. The addition of water also enhanced grain growth and assisted in attainment of equilibrium. It is important to note that this approach is valid to constrain peak metamorphic conditions but sheds limited light on the retrograde evolution. During exhumation, only a limited amount of H_2O was present (otherwise anhydrous peak minerals would not have survived). The main aim of the

Table 4
Trace element compositions (ppm) of representative peak UHP and HP phases (sample: RPC609)

Mineral	Cpx core (5)	Cpx rim (5)	Grt core (6)	Grt rim (6)	Am	Am	Ilm	Ap
Li	12.5	6.86	0.46	0.36	0.83	1.38	0.07	1.71
Be	0.78	0.59	Bdl	Bdl	7.33	6.20	0.01	0.00
P	14.7	16.9	260	167	60.4	35.8	8.83	–
K	32.8	32.0	Bdl	Bdl	24.3	56.6	1.23	9.65
Sc	25.8	34.6	68.8	66.2	50.5	42.0	15.2	7.70
Ti	461	459	494	240	–	–	–	139
Cr	265	312	134	222	313	347	69.2	0.00
Ni	346	282	6.27	6.73	383	325	184	0.00
Rb	0.12	0.23	0.04	Bdl	0.09	0.13	0.00	0.08
Sr	955	830	0.60	0.15	386	344	N.A.	7578
Y	1.34	5.64	65.8	38.6	31.9	11.3	1.07	32.0
Zr	7.45	10.0	12.2	9.23	28.7	28.7	118	1.68
Nb	0.01	0.01	0.57	0.01	6.50	6.19	66.48	0.01
Cs	0.01	0.05	Bdl	Bdl	0.00	0.00	0.00	0.04
Ba	109	28.9	0.03	Bdl	2.14	14.0	0.62	7.63
La	5.82	4.61	0.04	0.03	4.45	2.85	0.03	583
Ce	22.9	19.8	0.19	0.12	17.6	13.0	0.06	1702
Pr	3.89	3.45	0.06	0.05	2.69	2.36	0.01	229
Nd	17.5	15.8	1.03	0.91	11.7	11.9	0.03	862
Sm	4.37	4.19	1.89	1.76	4.15	4.13	0.02	133
Eu	1.08	1.11	1.13	1.07	1.87	1.42	0.01	26.0
Gd	2.33	2.75	6.05	5.12	6.33	3.91	0.05	64.2
Tb	0.17	0.28	1.36	0.99	1.00	0.48	0.01	3.91
Dy	0.52	1.29	11.0	7.05	6.49	2.61	0.12	11.5
Er	0.08	0.49	7.87	4.56	3.43	1.23	0.14	2.24
Yb	0.04	0.40	8.16	4.66	3.07	1.22	0.34	1.26
Lu	0.00	0.06	1.19	0.71	0.44	0.17	0.07	0.18
Hf	0.58	0.84	0.19	0.13	0.83	1.20	2.70	0.11
Ta	Bdl	Bdl	0.12	Bdl	0.16	0.17	4.45	0.00
Pb	12.9	8.85	0.13	0.08	13.4	9.69	0.04	8.92
Th	0.03	0.02	Bdl	Bdl	0.02	0.00	0.00	6.37
U	0.01	0.00	Bdl	Bdl	0.03	0.01	0.00	2.10

Trace element compositions of clinopyroxene and garnet are expressed as average.
In brackets is the number of representative analyses considered. N.A.=not analysed,–=stoichiometric.

experiments are thus threefold: 1) establish whether or not quartz or coesite can be stable in such bulk systems; 2) define a stability field for the peak metamorphic assemblage garnet, clinopyroxene and rutile; and 3) obtain the primary compositions for garnet and clinopyroxene to better constrain the observed formation of oriented needles with various compositions in these minerals.

7.2. Phase relations

The experimental conditions and the corresponding phase assemblages observed are listed in Table 5. Most of the experiments produced well-crystallised solid phases (Fig. 8), with euhedral to subhedral crystal shapes and average grain size ranging from <5 to 20 μm. In the investigated pressure–temperature range (1.5–3.5 GPa and 700–900 °C), garnet, clinopyroxene and amphibole are the major mineral constituents. Neither quartz nor coesite was found in any experiment. Rutile is present as accessory phase in all experiments, except one 1.5 GPa experiment where titanite was found.

The 3.5 GPa experiments were run at 700–800–900 °C. All these experiments produced a stable paragenesis characterised by the presence of garnet + clinopyroxene + rutile (Fig. 9). Garnet is always idioblastic and homogeneously distributed in the experimental charge, whereas clinopyroxene is idiomorphic to sub-idiomorphic and forms a fine-grained matrix around larger garnet grains (Fig. 8A, B and C). At 3.5 GPa and 700 °C orthopyroxene appears in equilibrium with clinopyroxene forming triple junctions in the matrix (Fig. 8A), whereas in the 800–900 °C runs orthopyroxene is missing in the clinopyroxene + garnet + rutile assemblage (Fig. 8B and C).

At 2.5 GPa, two runs at 700 and 800 °C were performed. In both experiments amphibole appeared as a stable phase coexisting with garnet, rutile and, to a lesser extent, with clinopyroxene (Fig. 9). Idioblastic garnet is stable at both run temperatures (Fig. 8D and E). At 700 °C garnet includes very small grains of epidote and is surrounded by a finer grain-sized amphibole ± clinopyroxene matrix. Amphibole is idioblastic, whereas clinopyroxene is sub-idioblastic to xenoblastic (Fig. 8D). At 2.5 GPa and 800 °C epidote disappears and garnet is stable with amphibole + clinopyroxene ± orthopyroxene.

Finally, one run at 1.5 GPa and 800 °C did not produce any clinopyroxene and garnet (Fig. 9). The paragenesis is constituted by amphibole, which occurs as well crystallised idioblasts, and by very fine-grained apatite and titanite distributed throughout the charge (Fig. 8F).

7.3. Phase compositions

Some representative average mineral compositions are reported in Table 6. Garnet displays a notable TiO_2-zoning with cores showing higher values (up to 2 wt.%) than rims (~0.8 wt.%). The rim compositions of several garnet grains, however, display more constant TiO_2 contents and the following data presentation is based on average composition of such rims. All runs at 3.5 GPa produced garnet

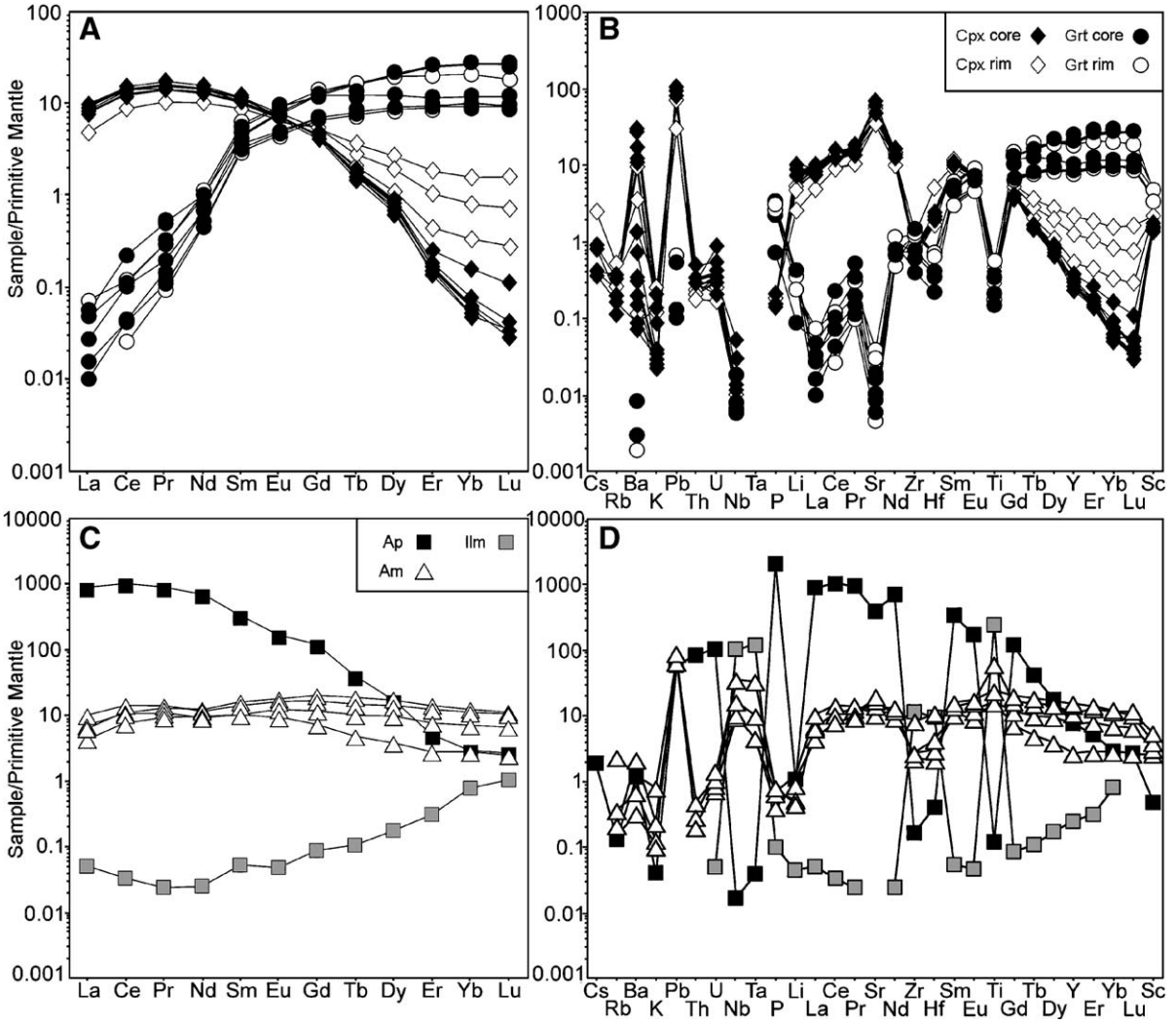

Fig. 7. Primitive mantle normalised REE and other trace element plots of peak minerals (A and B) and post-peak minerals (C and D). Normalising values after McDonough and Sun (1995).

consisting of 20–30 mol.% grossular, 30–37 mol.% almandine and 35–48 mol.% pyrope. The almandine content of garnet slightly increases with decreasing pressure; at 2.5 GPa and 700 °C garnet may contain up to 45–46 mol.% almandine. The MgO and FeO content of experimental garnets are comparable to the garnet composition seen in natural samples. The exception being CaO, which is slightly higher in experimental garnet relative to garnet in the eclogites (Table 6). Experimental garnet is buffered with rutile and is characterised by generally high TiO_2 (0.7–0.85 wt.%). This is much higher than the values measured in the natural garnet, even after integrating the segregated Ti-phases. There is a weak tendency for an increase in TiO_2 content with increasing pressures. Garnet is also characterised by clearly detectable Na_2O in the highest-grade conditions, and by the presence of detectable P_2O_5, in some experiments.

The experimental clinopyroxene is smaller and more homogeneous than garnet, and mainly corresponds to diopside and augite (Morimoto, 1989). It shows higher Al_2O_3, Na_2O and TiO_2 contents than natural clinopyroxene of the three studied samples. Al_2O_3 and FeO decrease with increasing temperature and pressure. TiO_2 contents are about a two- to three-factors lower than in garnet, but still significantly higher than in the natural samples. The K_2O content in experimental clinopyroxene is very low

Table 5
Experimental run conditions and products

P (GPa)	*T* (°C)	Time (h)	wt.% H_2O	Phases
3.5	900	165	5	Cpx, Grt, Rt
2.5	800	166	5	Cpx, Am, Grt, ±Opx, Rt
1.5	800	163	5	Am, Ttn, ±Ap, ±Grt
3.5	700	140	5	Cpx, Grt, Opx, Rt
2.5	700	260	5	Am, Grt, Ep, Rt, ±Cpx
3.5	800	166	5	Cpx, Grt, Rt

h=hours.

(<0.02 wt.%), due to the very low potassium content of the starting material (Table 1).

Experimental amphibole composition appears to vary significantly with changing *P–T* conditions. According to the nomenclature of Leake et al. (1997), amphibole produced at 2.5 GPa and 700–800 °C is actinolitic hornblende, edenite and Mg-hornblende. The TiO_2 content of amphibole at 2.5 GPa appears to increase with an increase in *T* from 700 to 800 °C. At 1.5 GPa and 800 °C amphibole composition corresponds to tschermakitic hornblende.

8. Discussion

8.1. Evidence for UHP metamorphism and implications for P–T evolution

The first identification of high-pressure metamorphism in the NDC was by Tsai and Liou (2000) who reported SiO_2 lamellae in omphacitic clinopyroxene of retrogressed eclogites from Raobazhai. They interpreted these oriented SiO_2 needles as quartz exsolutions from former Ca–eskola-bearing supersilicic clinopyroxene stable at pressures above 2.5 GPa. They estimated the eclogite-facies temperatures in the range of 800–820 °C, using Fe–Mg exchange geothermometers between garnet and included clinopyroxene. However, Tsai and Liou (2000) emphasised that these temperatures are not well constrained

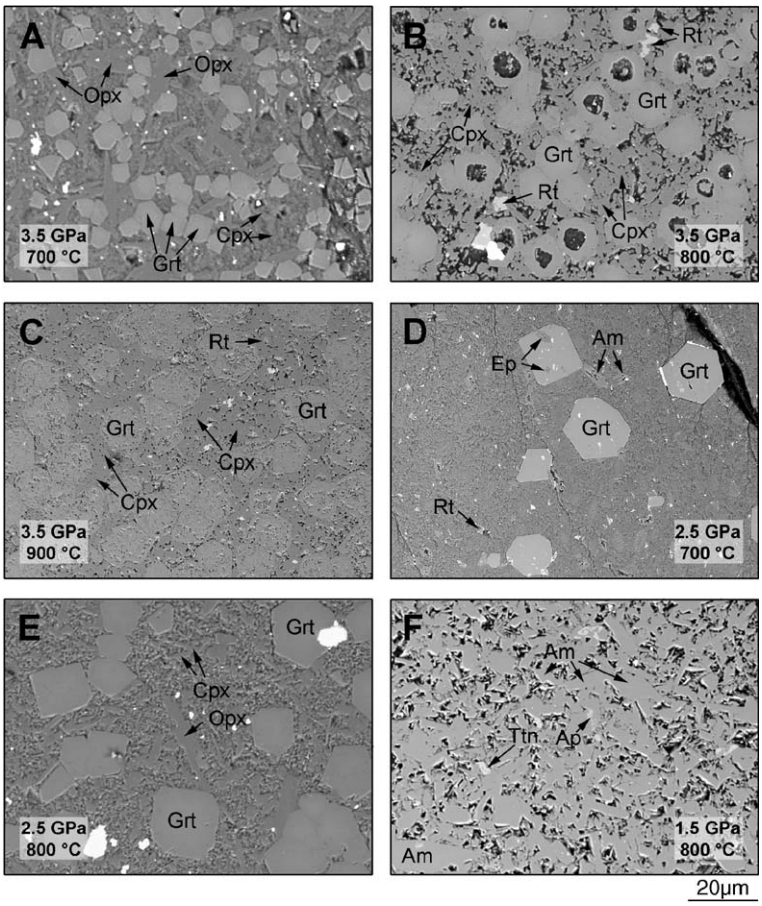

Fig. 8. Back scattered electron images of the experimental mineral assemblages. The different run conditions are shown in the lower corners of every picture.

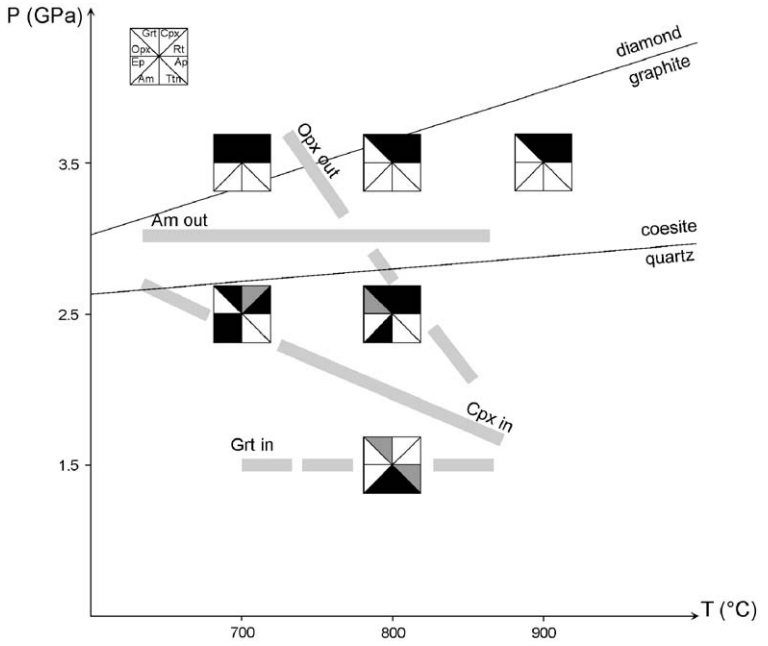

Fig. 9. *P–T* diagram reporting the experimental results together with the quartz–coesite and graphite–diamond transitions. Major and accessory phases are shown in black and in grey, respectively. The shaded lines display the limits of the stability fields for garnet, amphibole and orthopyroxene in the investigated system.

due to the thermal re-equilibration of these eclogites during retrograde metamorphism. The same Fe–Mg exchange geothermometers (Ellis and Green, 1979; Krogh, 1988; Krogh, 2000) applied to samples RPC608, RPC609 and RPC610 yield a large scatter of temperature values. These thermometers do not give reliable results because of post-peak major element re-equilibration in garnet. This is exceptionally well documented in the studied samples by the homogeneous major element compositions of garnet cores and rims (Fig. 6). The textural observations suggest that only the core domain, which contains rutile inclusions, was stable at the UHP peak and that the garnet rim grew during the HP_1 stage. The indistinguishable composition of core and rim provides evidence that the whole garnet composition must have equilibrated during decompression. The major element composition of lamellae-rich core domains in clinopyroxene is identical to the composition of small clinopyroxene inclusions in garnet rims. This observation indicates that peak metamorphic composition is not preserved in clinopyroxene. A further complication arises in that clinopyroxene rims are not in trace element equilibrium with garnet (Fig. 7). Hence garnet-clinopyroxene thermometry can not be applied to rim compositions. This study highlights how difficult it is to evaluate peak metamorphic conditions in eclogite-facies rocks when they are exposed to granulite-facies conditions during exhumation, which leads to homogenisation of mineral compositions via diffusion.

The experimental work, together with microstructural observations and trace element mineral compositions help to constrain the peak event of the studied NDC eclogites. In these rocks the peak assemblage is garnet+clinopyroxene+rutile (Fig. 3). The experiments show that in the investigated *P–T* range this anhydrous paragenesis is stable at $P>2.5$ GPa, above the stability field of amphibole (Fig. 9). At these pressure conditions the phase diagram of Fig. 9 identifies two possible parageneses: (i) orthopyroxene+garnet+clinopyroxene+rutile at $T<800$ °C; and (ii) garnet+clinopyroxene+rutile (orthopyroxene free) at $T=800$–900 °C. These phase relations constrain the peak temperature conditions at above 700 °C. The comparison between experimental products and sample petrography, and between major element compositions of experimental phases and of rock forming minerals, enabled us to conclude that the NDC eclogites most likely underwent UHP metamorphism at $P\sim3.5$ GPa and $T\geq750$–800 °C. The experimental run at 3.5 GPa and 900 °C did not produce any melt phase, thus indicating that the solidus of the studied rock system likely lies above 900 °C. The experimental work of Okamoto and Maruyama (1998) demonstrated that

Table 6
Major element average compositions (wt.%) and structural formulae of representative experimental products

P (GPa)–T (°C)	3.5–700	3.5–800	3.5–900	2.5–800	3.5–700	3.5–800	3.5–900	2.5–700	2.5–800	3.5–700	2.5–800	2.5–800	1.5–800
Mineral	Cpx (5)	Cpx (3)	Cpx (5)	Cpx (5)	Grt (5)	Grt (4)	Grt (10)	Grt (4)	Grt (4)	Opx (4)	Opx (2)	Am (5)	Am (4)
SiO_2	56.33	54.43	54.75	53.35	39.55	40.11	41.07	39.01	39.98	55.56	53.05	49.07	44.53
TiO_2	0.20	0.38	0.27	0.33	0.79	0.75	0.84	0.74	0.73	0.06	0.08	0.61	1.13
Al_2O_3	6.67	6.44	3.92	4.48	23.11	22.20	21.33	21.92	22.16	2.11	2.51	9.33	14.30
Cr_2O_3	0.03	0.12	0.14	0.09	0.09	0.09	0.09	0.10	0.17	0.05	0.03	0.07	0.07
FeO	4.17	4.98	6.07	5.71	17.43	16.54	17.06	21.74	18.31	10.96	16.50	7.61	12.57
MgO	13.97	13.40	14.28	14.76	10.11	12.18	12.51	6.06	10.44	29.53	25.37	16.65	12.65
MnO	0.05	0.03	0.09	0.04	0.19	0.20	0.23	0.56	0.55	0.05	0.21	0.06	0.14
CaO	16.77	17.36	18.29	19.78	9.79	9.03	8.32	11.35	8.20	0.95	1.49	10.74	11.02
Na_2O	3.60	3.02	2.43	1.95	0.07	0.36	0.27	Bdl	Bdl	0.27	0.13	2.74	1.47
K_2O	0.01	0.02	0.01	0.01	Bdl	Bdl	Bdl	Bdl	Bdl	Bdl	Bdl	0.07	0.03
P_2O_5	Bdl	Bdl	Bdl	Bdl	0.09	0.04	0.06	0.11	Bdl	Bdl	Bdl	Bdl	Bdl
Total	101.80	100.19	100.24	100.50	101.20	101.49	101.77	101.60	100.54	99.53	99.37	96.95	97.92
Si	1.97	1.96	1.97	1.94	2.93	2.93	3.00	2.96	2.99	1.97	1.93	6.98	6.40
Ti	0.01	0.01	0.01	0.01	0.04	0.04	0.05	0.04	0.04	0.00	0.00	0.07	0.12
Al	0.28	0.27	0.17	0.19	2.02	1.91	1.84	1.96	1.95	0.09	0.11	1.56	2.42
Cr	0.00	0.00	0.00	0.00	0.01	0.01	0.01	0.01	0.01	0.00	0.00	0.01	0.01
Fe^{2+}	0.12†	0.15†	0.18†	0.17†	1.06	0.83	0.95	1.37	1.15	0.32	0.47	0.72	1.20
Fe^{3+}					0.02	0.19	0.09	0.01	0.00	0.00	0.03	0.18	0.31
Mg	0.73	0.72	0.77	0.80	1.12	1.33	1.36	0.68	1.16	1.56	1.38	3.53	2.71
Mn	0.00	0.00	0.00	0.00	0.01	0.01	0.01	0.04	0.03	0.00	0.01	0.01	0.02
Ca	0.63	0.67	0.71	0.77	0.78	0.71	0.65	0.92	0.66	0.04	0.06	1.64	1.70
Na	0.25	0.21	0.17	0.14	0.01	0.05	0.04	Bdl	Bdl	0.02	0.01	0.75	0.41
K	0.00	0.00	0.00	0.00	Bdl	Bdl	Bdl	Bdl	Bdl	Bdl	Bdl	0.01	0.00
P	Bdl	Bdl	Bdl	Bdl	0.01	0.00	0.00	0.01	Bdl	Bdl	Bdl	Bdl	Bdl
Cation sum	3.99	3.99	3.98	4.02	8.00	8.00	8.00	8.00	8.00	4.00	4.00	15.46	15.31

Clinopyroxene and amphibole are normalised on the basis of 6 oxygens and 23 oxygens, respectively. Garnet is normalised on the basis of 8 cations and 12 oxygens; orthopyroxene is normalised on the basis of 4 cations and 6 oxygens. Fe^{3+} calculation for garnet and orthopyroxene as in Table 2.
†=Total iron as Fe^{2+}. Number in brackets refers to analyses used for the average.

eclogitic rocks, with 0.31 wt.% K_2O, from a diamondiferous locality in the Dabie Mountains (Xu et al., 1992; Okay, 1993) may melt at T=1100 °C at 3.5 GPa. This temperature value can be considered as a maximum temperature for the stability of our UHP assemblage.

Post-peak transformations (Fig. 3) are represented by the segregation of quartz+K-feldspar+albite in clinopyroxene and of rutile+ilmenite in garnet caused by a pressure–temperature decrease during exhumation from UHP to HP conditions (as will be discussed later). At this HP_1 stage, apatite is included in the garnet rims and stably coexists with garnet and clinopyroxene. This is shown in Fig. 7C, where apatite displays HREE depletion, indicating equilibrium partitioning with garnet during its growth. The stage HP_1 is followed by rock hydration with crystallisation of pargasitic amphibole (stage HP_2). Similarly to the clinopyroxene rims, pargasitic amphibole displays a flat REE pattern, indicating formation outside the garnet stability field (Fig. 7D). According to the experimental results of Fig. 9, in the presence of a fluid phase garnet is only stable above 1.5 GPa. Hence we suggest that the retrograde HP_2 stage likely occurred at pressures lower than 1.5 GPa. The latest retrograde stage features the formation of orthopyroxene+spinel+plagioclase+amphibole symplectites at the expenses of garnet (Fig. 2F), indicating fluid-assisted recrystallisation at granulite-facies conditions.

8.2. Origin of lamellae in clinopyroxene and garnet

8.2.1. Quartz+K-feldspar+albite in clinopyroxene

The occurrence of oriented lamellae is a common feature of minerals that derive from deep-seated sources such as kimberlites, diamondiferous rocks, as well as in eclogites and ultramafites from UHP metamorphic belts. Quartz oriented needles and/or K-feldspar lamellae in clinopyroxene have been described by several authors (Smith, 1984; Shatsky et al., 1985; Sobolev and Shatsky, 1990; Bakun-

Czubarow, 1992; Gayk et al., 1995; Zhang et al., 1995; Perchuk et al., 1996; Zhang et al., 1997; Nakajima and Ogasawara, 1998; Liou et al., 1998; Tsai and Liou, 2000; Bruno et al., 2002; Perchuk et al., 2002). Silica and K-feldspar rods are considered to be segregation products from pre-existing supersilicic and K-rich clinopyroxene, respectively, that contained excess SiO_2 or K_2O at peak metamorphic conditions (Smith, 1984; Zhang et al., 1997; Zhang and Liou, 2000; Perchuk et al., 2002). The observed lamellae in clinopyroxene of our samples likely represent such segregations derived from a supersilicic, K- and Na-rich pyroxene. Alternatively the mineral association quartz+K-feldspar+albite might derive from crystallisation of a trapped melt generated by the subducting crust. The observation that lamellae are crystallographically oriented suggests that they correspond to segregations from a previous omphacitic pyroxene. The proportion of feldspars to quartz varies among different inclusions, a feature that would not be expected if the oriented precipitates represent trapped melts. Laser Ablation analyses of clinopyroxene cores have been carried out with a spot size of 180 μm to qualitatively define the trace element composition of clinopyroxene+lamellae and thus infer the composition of the original UHP clinopyroxene. The analytical results (Table 4) show that clinopyroxene cores (corresponding to mixtures of clinopyroxene +lamellae) are not enriched in LREE and other incompatible elements with respect to lamellae-free domains, which would be expected by the occurrence of melt inclusions (Adam et al., 1997; Hermann and Green, 2001; Hermann, 2002). This enables us to rule out that inclusions are entrapped silicate melts. We conclude that the oriented needles in clinopyroxene are segregations derived from a previous Na_2O- and SiO_2-rich UHP clinopyroxene.

Despite the very low K-content of clinopyroxene, the occurrence of K-feldspar lamellae provides evidence that K was incorporated in clinopyroxene prior to or during the UHP metamorphism. The composition of UHP clinopyroxene in the studied rocks was achieved by integrating feldspar and quartz lamellae with the clinopyroxene core-compositions (Table 3). The compositions obtained are in good agreement with clinopyroxene compositions observed in experimental runs at pressures of 3.5 GPa (Table 6). Segregation-bearing natural clinopyroxene and the experimental clinopyroxene display higher Na_2O concentrations and higher SiO_2/CaO ratios than lamellae-free domains. The high SiO_2/CaO, particularly in experimental clinopyroxene, may be indicative of the presence of 1–3% of Ca–eskola component, calculated following Katayama et al. (2000). We suggest that the absence of quartz during prograde and peak metamorphic conditions might have promoted the incorporation of K in clinopyroxene. K substitutes for Na in the M_1 site of the jadeite molecule (Jd), forming a $KAlSi_2O_6$ component in clinopyroxene. This component is stabilised with respect to K-feldspar or phengite in an environment with low SiO_2 activity.

The relative timing of segregation can be constrained by textural observations. Garnet rims, formed during the stage HP_1, contains clinopyroxene inclusions lacking lamellae and with a composition very similar to the clinopyroxene core (Table 2). This provides evidence that the lamellae formed during decompression from the UHP to HP_1 stage (Fig. 3). The Ca–eskola component breaks down during decompression through the reaction: $2Ca_{0.5}\square_{0.5}AlSi_2O_6 \rightarrow CaAl_2SiO_6 + 3SiO_2$ (Katayama et al., 2000; Bruno et al., 2002). This reaction causes segregation of oriented quartz needles and an increase of the Ca–Tschermak component in the newly formed clinopyroxene. The presence of free SiO_2 enables the precipitation of K-feldspar ($KAlSi_2O_6 + SiO_2 = KAlSi_3O_8$) and albite ($Jd + SiO_2 = NaAlSi_3O_8$) from the K and Na component in clinopyroxene. The segregation of considerable amounts of albite changes the clinopyroxene composition from omphacitic to diopsidic, as showed in Table 2. In summary, the combined approach of this study using textures, mineral trace element compositions and experimental compositions provides evidence that the observed lamellae are segregations, that form from a supersilicic, K-bearing clinopyroxene during decompression from UHP to HP conditions.

8.2.2. Ilmenite+rutile in garnet

Oriented rutile rods segregated from garnet have been recognised in eclogites and garnet-pyroxenites from UHP Sulu terrane (Zhang et al., 1994; Ye et al., 1997; Zhang and Liou, 1998; Zhang and Liou, 1999; Ye et al., 2000; Zhang et al., 2003) and in eclogites from the Western Gneiss Region, Norway (Smith, 1988). Some experiments on Ti solubility in garnet and clinopyroxene were carried out by Zhang et al. (2003) who used a garnet-clinopyroxenite from Sulu as starting material. Their experiments were performed at 5.0–15 GPa and 1000–1400 °C and indicate that Ti solubility in garnet is positively correlated with pressure. Our experimental results show that it is not necessary to have such extreme metamorphic conditions to form Ti-rich garnet. Garnet formed during experimental runs at 3.5 GPa and 700–800–900 °C has very high Ti contents of about 4800 ppm (Table 6), which is much higher than that of natural

garnet in sample RPC609 showing rutile rods. Laser Ablation analyses of garnet cores (corresponding to garnet+rods) yield maximum values of ~670 ppm. The comparison of Ti content of experimental garnet with the Ti measured in natural garnet indicates that the latter lost some Ti before formation of segregations or during the post-peak re-equilibration. This suggests that some of the Ti now hosted in retrograde ilmenite was originally incorporated in the structure of the peak metamorphic garnet (that changed composition during exhumation). It is important to note that even garnet formed in experiments at 2.5 GPa contains relatively high Ti contents. Therefore, it seems that rutile segregation in garnet is not a diagnostic feature of garnet originating from UHP conditions.

8.3. Multiple stages of metasomatism

8.3.1. Nature of the protolith

Prior to assessing changes related to metasomatism, the nature of the protolith needs to be constrained. The bulk-rock major element and REE compositions of RPC608, RPC609 and RPC610 indicate that they derive from a mafic protolith (Table 1; Figs. 4 and 5A). The first question to address is whether the investigated rocks have a gabbroic or basaltic protolith. The CaO and Al_2O_3 contents of the mafic rocks are very close to values for the plotted basaltic reference compositions (Fig. 4). This indicates that only a limited amount of cumulus plagioclase was present in the sample. This is further supported by the REE patterns (Fig. 5A) that do not show any positive Eu-anomaly, which is typical for accumulated plagioclase (Hermann et al., 2001). Moreover, the trace element patterns of the studied mafic rocks (Fig. 5B) show remarkably similar patterns to basalts and do not show significant contamination by cumulus pyroxene or olivine. All these observations provide evidence that the major and trace element composition of the investigated rocks is dominated by a frozen melt composition (e.g. Hermann et al., 2001) and hence the rocks can be compared to basalts from different settings.

The trace element patterns of the studied samples are compared in Fig. 5 with MORB (tholeiitic affinity) and continental basalts (alkaline affinity). The latter have been proposed as protoliths of other eclogites of NDC (Rumble et al., 2004 and references therein; Liu et al., 2005). The normalised REE concentrations of eclogites studied in this work largely overlap with the reference MORB pattern, particularly the least differentiated sample RPC608 (Fig. 5A). Moreover, Fig. 5B emphasises that fluid immobile elements – such as Nb, Ta, Zr, Hf, Ti, HREE, and Sc – in the studied rocks closely match the concentrations of the average MORB. In contrast, when compared to the continental basalts the investigated primitive samples have lower Th, Nb, Ta and LREE contents. As a consequence, we propose that our NDC eclogites derive from a protolith with tholeiitic character. This does not necessitate that the Shan Guan Tuan mafic–ultramafic complex represents a remnant of oceanic crust. Similarly to continental basalts, tholeiitic igneous rocks have also been described in continental settings (Hansmann et al., 2001; Hermann et al., 2001).

With respect to a reference MORB composition RPC608, RPC609 and RPC610 show significant variations. Their major element composition indicates considerable depletion in SiO_2 and alkalis and enrichment in MgO and FeO (Fig. 4). These features suggest element exchange with Si-depleted and Mg-enriched systems, such as the hosting ultramafic rocks. On the other hand, the trace element bulk-rock signature of the investigated samples shows a marked enrichment in fluid–mobile elements (Fig. 5B). Such elements generally reside in continental crustal rocks and are unlikely sourced from ultramafic systems. These contrasting fingerprints thus require interaction with metasomatic agents sourced by different rock systems, likely corresponding to ultramafic and crustal reservoirs. It is possible that the analysed NDC eclogites represent hybrid rock types which record metasomatic exchanges that occurred during different stages of their metamorphic history.

8.3.2. Low-grade metasomatism

Fig. 4 shows that the major element compositions of investigated samples are intermediate between ultramafic and basaltic systems. Compared with average major element contents of basaltic rocks, the NDC samples display lower SiO_2 and Na_2O, and higher MgO and $Fe_2O_{3_{tot}}$. The timing of silica depletion must have been prior to growth of metamorphic garnet because no quartz inclusions have been found. This is in agreement with experiments, which demonstrate that for all investigated conditions, no free SiO_2 phase was stable. Si-depleted and Mg-enriched compositions can be obtained by the influx of fluids, which assisted low-grade alteration and serpentinisation of the eclogite-hosting ultramafics. Interaction of such a fluid with mafic systems resulted in a Mg-metasomatism, which was coupled with appreciable silica loss. Comparable features, first described for metasomatised gabbroic layers in serpentinites from HP Alpine ophiolites (Scambelluri and Rampone, 1999), were recently advocated to explain the compositional variations of

Ti-clinohumite-bearing metagabbros from the Sulu ultramafic complex (Yang, 2003). In both occurrences, starting gabbroic materials were depleted in CaO and SiO_2 and enriched in MgO as the result of fluid mediated element exchange between serpentinising peridotites and gabbros at low metamorphic grade in oceanic and/or shallow crustal environments.

8.3.3. HP/UHP metasomatism

The bulk-rock trace element composition of RPC608, RPC609 and RPC610 is enriched in the fluid–mobile elements Cs, Ba, Pb and Sr (Fig. 5B). To understand the main chemical changes that occurred to the studied samples, the trace element patterns of the least retrogressed samples RPC608 and RPC609 have been normalised to the estimated protolith rock, i.e. average N-MORB (Fig. 10). Compared with such N-MORB, the studied samples display selective enrichment in fluid–mobile elements, indicating interaction with a LILE- and Sr-rich metasomatic agent. In Fig. 10 the trace element patterns of RPC608 and RPC609 are also compared with a range composition of altered sea-floor basalts (data from Staudigel et al., 1996; Alt and Teagle, 2003), characterised by spikes of Rb, K, U, depletion in Th, strong Nb/Ta fractionation and negative Sr anomaly. The trace element pattern of altered basalts is quite different from that of NDC eclogites: this indicates that the observed metasomatic signature is neither produced by the Mg-metasomatism discussed above, nor by a low-grade sea-floor alteration of precursor basalts. In Fig. 10 the trace element composition of the average Upper Crust (Taylor and McLennan, 1995) and Central East China and Yangtze Craton crust (Gao et al., 1998) are also reported. The various patterns of crustal rocks are all similar and show the progressive enrichment in the most incompatible elements and LILE with respect to the reference N-MORB. These patterns, compared with the ones of RPC608 and RPC609, show similar LILE and fluid–mobile element enrichment. We can therefore assume that the LILE- and Sr-enrichment in the investigated eclogites was produced by the influx of fluids sourced by a crustal reservoir. The relative depletion of Rb and K with respect to Ba and Cs indicates that phengite was present in the crustal reservoir at the time of fluid extraction because phengite preferentially partitions Rb and K with respect to other LILE (Melzer and Wunder, 2000).

The analysis of such elements in the rock-forming minerals and their incorporation in a given mineral paragenesis make it possible to identify timing of crustal metasomatic fluid infiltration in these rocks. A LILE- and Sr-enriched geochemical signature pertains to the peak UHP clinopyroxene (Fig. 7B), thus indicating that the crustal element influx occurred prior to, or synchronous with the UHP recrystallisation. Further

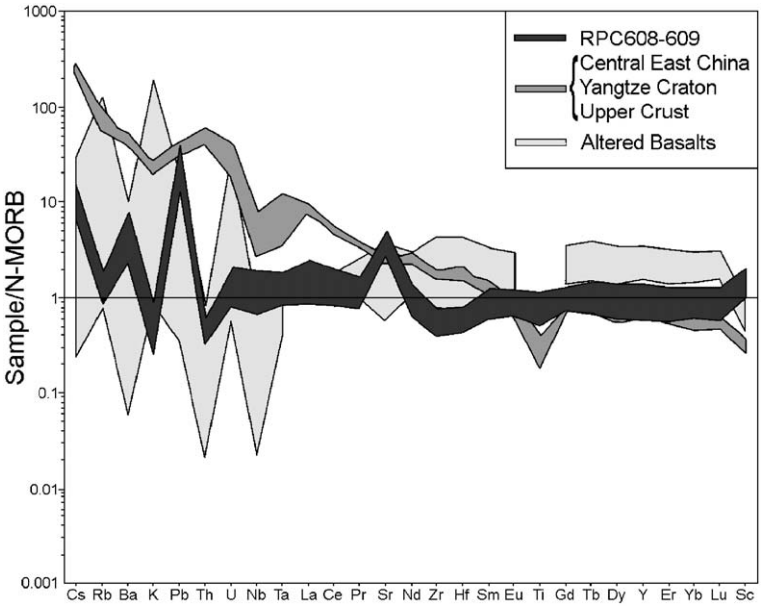

Fig. 10. N-MORB normalised bulk-rock trace elements plots. N-MORB from Hofmann (1988); crustal compositions are averages among Central East China, Yangtze Craton (both from Gao et al., 1998) and Upper Crust (Taylor and McLennan, 1995); altered basalts are an average between data from Staudigel et al. (1996), and Alt and Teagle (2003).

evidence for this includes the presence of Ba-bearing feldspar lamellae (Table 3), showing that Ba uptake occurred during the prograde or peak metamorphism. Moreover, the LILE contents in the UHP clinopyroxene are much higher than the concentrations in post-peak HP mineral phases like amphibole (Fig. 7D), which is supposed to be the best candidate to host these elements (Adam et al., 1997; Najorka et al., 1999). All these features indicate that the LILE- and Sr-metasomatism, produced by crustal fluid influx, occurred during subduction at HP/UHP metamorphic conditions.

8.3.4. Metasomatism in coupled mafic–ultramafic rocks

The petrologic and geochemical features of the NDC eclogites presented here are gathered into a speculative model that possibly explains the multistage metasomatism affecting these rocks. This work provides the "best guess" of these processes in light of the limited exposure. The observed multistage metasomatism in the NDC rocks can be explained in a model based on the coupling of felsic, mafic and ultramafic rocks during subduction and exhumation (Fig. 11). The first stage recognised (box 1, Fig. 11) features the influx of Si-undersaturated and Mg-enriched fluids, likely sourced from the associated harzburgitic and lherzolitic rocks undergoing a serpentinisation process. This metasomatism likely occurred at low-grade metamorphic conditions, within the stability field of serpentine, and represents an early pre-subduction feature. The second stage of metasomatism (box 2, Fig. 11) was accompanied by the influx of fluids transporting LILE and Sr. Since this fluid was probably sourced from crustal units, this metasomatic stage likely marks the tectonic coupling of mafic–ultramafic rocks with continental crust. The background phase relations of Fig. 11 portrays the *P–T* stability fields of hydrous phases for a fluid-saturated lherzolite composition (Fumagalli and Poli, 2005). The meta-lherzolites hosting the NDC eclogites play a fundamental role in the overall fluid-mediated element transfer from the crustal units to the

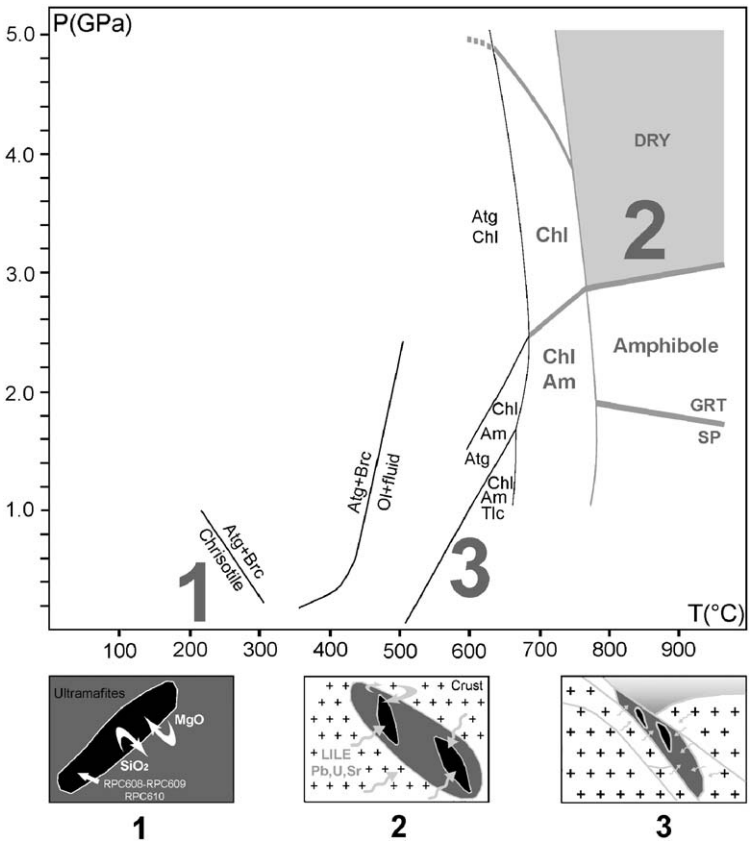

Fig. 11. *P–T* diagram showing a schematic representation of the possible multiple-stage metasomatism (numbers from 1 to 3) of RPC608, RPC609 and RPC610 during their evolution. See text for explanations. The stability fields of hydrous phases in the NCFMASH system are from Fumagalli and Poli (2005). Insets display the element exchanges during the various metasomatic events at different scales.

metasomatised eclogites. Enrichment in fluid mobile elements in the NDC eclogites implies that no significant LILE and trace element mineral repository (e.g. amphibole and/or phlogopite) was stable in the ultramafic hosts. This means that the metasomatic LILE enrichment of the NDC eclogites may have occurred above 2.5 GPa, i.e. the maximum pressure for amphibole stability in mafic and ultramafic systems (Poli, 1993; Fumagalli and Poli, 2005), and above 750–800 °C ("Dry" field, Fig. 11). The pressure range for the crust-derived metasomatism is therefore between 2.5 and 3.5 GPa, the pressure estimated for the UHP equilibration of the studied samples. This suggests that ultramafic rocks behaved as transparent media for fluids containing LILE and Sr, because there was no stable hydrous phase in the ultramafic rocks that could have interacted and changed the fluid composition. On the other hand, because much of the retrograde evolution occurred within the stability field of hydrous phases in ultramafic rocks, the peridotites hosting the eclogites acted as crustal fluid filters, preventing retrogression of the eclogites and further metasomatic changes. For example, during retrograde metasomatism at granulite- and amphibolite-facies conditions, estimated at 1.1–1.4 GPa and 800–900 °C (Xu et al., 2000; Liu et al., 2001; Xu et al., 2002), the associated crustal rocks likely produced fluid and/or partial melts (box 3, Fig. 11). At these conditions a free fluid phase, derived from the crustal rocks, would immediately interact with the peridotites and form hydrous phases such as amphibole. Retrograde amphibole that formed at 0.6–1.8 GPa has been described from peridotitic rocks hosting Raobazhai eclogites (Tsai et al., 2000). The formation of such amphibole prevents further infiltration of metasomatising agents inside the eclogites. This is documented in the NDC eclogites by the observation that the small amount of retrograde amphibole is much less enriched in trace elements than the peak clinopyroxene. We therefore conclude that eclogites hosted in ultramafic rocks have a much higher probability of preserving UHP metamorphism than eclogites directly hosted in gneisses.

Acknowledgements

This research was developed by N. Malaspina during her permanence at the Research School of Earth Sciences (ANU), Canberra. The technical assistance of W.O. Hibberson in the high-pressure laboratory and analytical assistance of A. Norris, C. Allan and M. Shelley at the Research School of Earth Sciences, and the help of L. Negretti for SEM analyses at the University of Genova are greatly acknowledged. Discussion with E. Rampone and F. Rolfo, and comments by N. Tailby, have been much appreciated. Critical reviews by C.H. Tsai and an anonymous reviewer helped to improve the manuscript. N. Malaspina and M. Scambelluri acknowledge funding by the Italian MIUR-Cofin to the project "Mass-transfer and role of fluids during peridotite emplacement in subducting continental crust: natural and experimental constraints". J. Hermann acknowledges financial support by the Australian Research Council and the Swiss National Science Foundation.

References

Adam, J., Green, T.H., Sie, S.H., Ryan, C.G., 1997. Trace element partitioning between aqueous fluids, silicate melts and minerals. European Journal of Mineralogy 9, 569–584.

Alt, J.C., Teagle, D.A.H., 2003. Hydrothermal alteration of upper oceanic crust formed at a fast-spreading ridge: mineral, chemical and isotopic evidence from ODP site 801. Chemical Geology 201, 191–211.

Bakun-Czubarow, N., 1992. Quartz pseudomorphs after coesite and quartz exsolutions in eclogitic omphacites of the Zlote Mountains in the Sudetes (SW Poland). Archiwum Mineralogiczne 48, 3–25.

Bebout, G.E., Ryan, J.G., Leeman, W.P., Bebout, A.E., 1999. Fractionation of trace elements by subduction-zone metamorphism; effect of convergent-margin thermal evolution. Earth and Planetary Science Letters 171, 63–81.

Becker, H., Jochum, K.P., Carlson, R.W., 2000. Trace element fractionation during dehydration of eclogites from high-pressure terranes and the implications for element fluxes in subduction zones. Chemical Geology 163, 65–99.

Brenan, J.M., Shaw, H.F., Ryerson, F.J., Phinney, D.L., 1995. Mineral–aqueous fluid partitioning of trace elements at 900 °C and 2.0 GPa; constraints on the trace element chemistry of mantle and deep crustal fluids. Geochimica et Cosmochimica Acta 59, 3331–3350.

Bruno, M., Compagnoni, R., Hirajima, T., Rubbo, M., 2002. Jadeite with the Ca–eskola molecule from the ultra-high pressure metagranodiorite, Dora Maira massif, Western Alps. Contributions to Mineralogy and Petrology 142, 515–519.

Bryant, D.L., Ayers, J.C., Gao, S., Miller, C.F., Zhang, H., 2004. Geochemical, age, and isotopic constraints on the location of the Sino-Korea/Yangtze Suture and evolution of the North Dabie Complex, east central China. Geological Society of America Bulletin 116, 698–717.

Bucher, K., Frey, M., 1994. Petrogenesis of Metamorphic Rocks. Springer-Verlag, Berlin. 318 pp.

Cong, B., Zhai, M., Zhao, Z., Carswell, D.A., Wilson, R.H., 1993. A typical area of UHP coesite-bearing eclogite and related rocks in Shuanghe Village, Dabie Mountains, central China; its petrology, metamorphic mineralogy and history, and evidence for collision and exhumation. In: Fourth international eclogite conference. Terra Abstracts 5 (Suppl. 4), 3–4.

Crocket, J.H., Paul, D.K., 2004. Platinum-group elements in Deccan mafic rocks: a comparison of suites differentiated by Ir content. Chemical Geology 208, 273–291.

Droop, G.T.R., 1987. A general equation for estimating Fe^{3+} concentrations in ferromagnesian silicates and oxides from microprobe analyses, using stoichiometric criteria. Mineralogical Magazine 51, 431–435.

Ellis, D.J., Green, D.H., 1979. An experimental study of the effect of Ca upon garnet-clinopyroxene Fe–Mg exchange equilibria. Contributions to Mineralogy and Petrology 71, 13–22.

Faure, M., Lin, W., Shu, L., Sun, Y., 1999. Structural constraints on the exhumation of ultra high-pressure rocks in Dabieshan (E. China). European Union of Geosciences Conference Abstracts, EUG 10Journal of Conference Abstracts, vol. 4; 1. Pages 42.

Faure, M., Lin, W., Scharer, U., Shu, L., Sun, Y., Arnaud, N., 2003. Continental subduction and exhumation of UHP rocks. Structural and geochronological insights from the Dabieshan (E China). Lithos 70, 213–241.

Fumagalli, P., Poli, S., 2005. Experimentally determined phase relations in hydrous peridotite to 6.5 GPa and their consequences on the dynamics of subduction zones. Journal of Petrology 46, 555–578.

Gao, S., Luo, T.C., Zhang, B.R., Zhang, H.F., Han, Y.W., Zhao, Z.D., Hu, Y.K., 1998. Chemical composition of the continental crust as revealed by studies in East China. Geochimica et Cosmochimica Acta 62, 1959–1975.

Gayk, T., Kleinschrodt, R., Langosch, A., Seidel, E., 1995. Quartz exsolution in clinopyroxene of high-pressure granulite from the Munchberg Massif. European Journal of Mineralogy 7, 1217–1220.

Hacker, B.R., Wang, X., Eide, E.A., Ratschbacher, L., 1996. Qinling–Dabie ultrahigh-pressure collisional orogeny. In: Yin, A., Harrison, T.M. (Eds.), The Tectonic Evolution of Asia. Cambridge University Press, Cambridge.

Hacker, B.R., Ratschbacher, L., Webb, L., Ireland, T., Walker, D., Dong, S., 1998. U/Pb zircon ages constrain the architecture of the ultrahigh-pressure Qinling–Dabie Orogen, China. Earth and Planetary Science Letters 161, 215–230.

Hacker, B.R., Ratschbacher, L., Webb, L., McWilliams, M.O., Calvert, A., Dong, S., Wenk, H.-R., Chateigner, D., 2000. Exhumation of ultrahigh-pressure continental crust in east-central China: Late-Triassic–Early Jurassic tectonic unroofing. Journal of Geophysical Research 105, 13339–13364.

Hansmann, W., Müntener, O., Hermann, J., 2001. U–Pb zircon geochronology of a tholeiitic intrusion and associated migmatites at a continental crust–mantle transition, Val Malenco, Italy. Schweizerische Mineralogische Und Petrographische Mitteilungen 81, 239–255.

Hermann, J., 2002. Allanite: thorium and light rare earth element carrier in subducted crust. Chemical Geology 192, 289–306.

Hermann, J., Green, D.H., 2001. Experimental constraints on high pressure melting in subducted crust. Earth and Planetary Science Letters 188, 149–168.

Hermann, J., Müntener, O., Günther, D., 2001. Differentiation of mafic magma in a continental crust-to-mantle transition zone. Journal of Petrology 42, 189–206.

Hirajima, T., Nakamura, D., 2003. The Dabie Shan–Sulu Orogen. EMU Notes in Mineralogy, vol. 5. Eötvös University Press, Budapest, pp. 105–144.

Hofmann, A.W., 1988. Chemical differentiation of the Earth: the relationship between mantle, continental crust and oceanic crust. Earth and Planetary Science Letters 90, 297–314.

Jahn, B.M., Wu, F., Lo, C.H., Tsai, C.H., 1999. Crust–mantle interaction induced by deep subduction of the continental crust: geochemical and Sr–Nd isotopic evidence from post-collisional mafic–ultramafic intrusions of the northern Dabie complex, central China. Chemical Geology 157, 119–146.

Katayama, I., Parkinson, C.D., Okamoto, K., Nakajima, Y., Maruyama, S., 2000. Supersilicic clinopyroxene and silica exsolution in UHPM eclogite and pelitic gneiss from the Kokchetav massif, Kazakhstan. American Mineralogist 85, 1368–1374.

Kogiso, T., Tatsumi, Y., Nakano, S., 1997. Trace element transport during dehydration processes in the subducted oceanic crust; 1, Experiments and implications for the origin of ocean island basalts. Earth and Planetary Science Letters 148, 193–205.

Krogh, E.J., 1988. The garnet-clinopyroxene Fe–Mg geothermometer — a reinterpretation of existing experimental data. Contributions to Mineralogy and Petrology 99, 44–48.

Krogh, E.J., 2000. The garnet-clinopyroxene Fe^{2+}–Mg thermometer: an updated calibration. Journal of Metamorphic Geology 18, 211–219.

Leake, B.E., et al., 1997. Nomenclature of amphiboles: report of the subcommittee on amphiboles of the International Mineralogical Association, commission on new minerals and mineral names. American Mineralogist 82, 1019–1037.

Lightfoot, P.C., Hawkesworth, C.J., Devey, C.W., Rogers, N.W., Van Calsteren, P., 1990. Source and differentiation of Deccan trap lavas: implications of geochemical and mineral variations. Journal of Petrology 31, 1165–1200.

Liou, J.G., Zhang, R.Y., Eide, E.A., Maruyama, S., Wang, X., Ernst, W.G., 1996. Metamorphism and tectonics of high-*P* belts in Dabie–Sulu Regions, eastern China. In: Yin, A., Harrison, T.M. (Eds.), The Tectonics Evolution of Asia. Cambridge Univ. Press, Cambridge, UK, pp. 300–343.

Liou, J.G., Zhang, R.Y., Ernst, W.G., Rumble, D., Maruyama, S., 1998. High-pressure minerals from deeply subducted metamorphic rocks. In: Hemley, R.J. (Ed.), Ultrahigh-Pressure Mineralogy: Physics and Chemistry of the Earth's Deep Interior. Reviews in mineralogy, vol. 37. Mineralogical Society of America, Washington.

Liu, Y., 2000. Petrology, geochemistry and isotopic chronology of the eclogites from the northern Dabie Mountains. PhD Thesis, University of Science and Technology of China, Hefei, China.

Liu, Y., Li, S., Xu, S., Li, H., Jiang, L., Chen, G., Wu, W., Su, W., 2000. U–Pb zircon ages of the eclogite and tonalitic gneiss from the northern Dabie Mountains, China and multi-overgrowths of metamorphic zircons. Geological Journal Chinese University 6, 417–423 (in Chinese with English abstract).

Liu, Y., Xu, S., Li, S., Chen, G., Jiang, L., Zhou, C., Wu, W., 2001. Distribution and metamorphic *P–T* conditions of the eclogites from the mafic–ultramafic belt in the northern part of the Dabie Mountains. Acta Geologica Sinica 75, 385–395 (in Chinese with English abstract).

Liu, Y.C., Li, S.G., Xu, S.T., Jahn, B.M., Zheng, Y.F., Zhang, Z. Q., Jiang, L.L., Chen, G.B., Wu, W.P., 2005. Geochemistry and geochronology of eclogites from northern Dabie Mountains, central China. Journal of Asian Earth Sciences 25, 431–443.

McDonough, W.F., 1991. Chemical and isotopic systematics of continental lithospheric mantle. In: Meyer, H.O.A., Leonardos, O.H. (Eds.), Kimberlites Related Rocks and Mantle Xenoliths. Companhia de Pesquisa de Recursos Minerais, Rio de Janeiro.

McDonough, W.F., Sun, S.S., 1995. Composition of the Earth. Chemical Geology 120, 223–253.

Melzer, S., Wunder, B., 2000. Island-arc basalt alkali ratios: constraints from phengite-fluid partitioning experiments. Geology 28, 583–586.

Morimoto, N., 1989. Nomenclature of pyroxenes. Canadian Mineralogist 27, 143–156.

Nakajima, Y., Ogasawara, Y., 1998. Petrology of eclogite and Ti-clinohumite bearing rock from Kumdykol, Kokchetav Massif, Kazakhstan—some mineralogical records of UHP conditions. Abstract of Japan Geological Society Spring Meeting, vol. 106, p. 52.

Najorka, J., Gottschalk, M., Franz, G., Heinrich, W., 1999. Ca–Sr distribution among amphibole, clinopyroxene and chloride-bearing solutions. American Mineralogist 84, 596–606.

Okamoto, K., Maruyama, S., 1998. Multi-anvil re-equilibration experiments of a Dabie Shan ultrahigh-pressure eclogite within the diamond-stability fields. Island Arc 7, 52–69.

Okay, A.I., 1993. Petrology of a diamond and coesite bearing metamorphic terrain: Dabie Shan, China. European Journal of Mineralogy 5, 659–673.

Okay, A.I., Xu, S., Sengor, A.M.C., 1989. Coesite from the Dabie Shan Eclogites, Central China. European Journal of Mineralogy 1, 595–598.

Okay, A.I., Sengor, A.M.C., Satir, M., 1993. Tectonics of an ultrahigh-pressure metamorphic terrane: the Dabieshan/Tongbaishan orogen, China. Tectonics 12, 1320–1334.

Pearce, N.J.G., Perkins, W.T., Westgate, J.A., Gorton, M.P., Jackson, S.E., Neal, C.R., Chenery, S.P., 1997. A compilation of new and published major and trace element data for NIST SRM 610 and NIST SRM 612 glass reference materials. Geostandards Newsletter 21, 115–144.

Peng, Z.X., Mahoney, J.J., Hooper, P.R., Macdougall, J.D., Krishnamurthy, P., 1998. Basalts of the northeastern Deccan Traps, India: isotopic and elemental geochemistry and relation to southwestern Deccan stratigraphy. Journal of Geophysical Research 103, 29843–29865.

Perchuk, L.L., Sobolev, N.V., Yapaskurt, V.O., Shatsky, V.S., 1996. Relics of potassium-bearing pyroxenes from diamond-free pyroxene-garnet rocks of the Kokchetav Massif, northern Kazakhstan. Doklady Rossikoi Akademii Nauk 348, 790–795.

Perchuk, L.L., Safonov, O.G., Yapaskurt, V.O., Barton Jr., J.M., 2002. Crystal-melt equilibria involving potassium-bearing clinopyroxene as indicator of mantle-derived ultrahigh-potassic liquid: an analytical review. Lithos 60, 89–111.

Poli, S., 1993. The amphibolite-eclogite transformation: an experimental study on basalt. American Journal of Science 293, 1061–1107.

Rolfo, F., Compagnoni, R., Wu, W., Xu, S., 2004. A coherent lithostratigraphic unit in the coesite–eclogite complex of Dabie Shan, China: geologic and petrologic evidence. Lithos 73, 71–94.

Rumble, D., Liou, J.G., Jahn, B.M., 2004. Continental crust subduction and UHP metamorphism. Treatise on Geochemistry, vol. 3. Chap. 3.09. Elsevier, Amsterdam, pp. 293–319.

Scambelluri, M., Philippot, P., 2001. Deep fluids in subduction zones. Lithos 55, 213–227.

Scambelluri, M., Rampone, E., 1999. Mg-metasomatism of oceanic gabbros and its control on Ti-clinohumite formation during eclogitization. Contributions to Mineralogy and Petrology 135, 1–17.

Schilling, J.G., Zajac, M., Evans, R., Johnston, T., White, W.M., Devine, J.D., Kingsley, R.H., 1983. Petrologic and geochemical variations along the Mid Atlantic Ridge from 29°N to 73°N. American Journal of Science 283, 510–586.

Schmidt, M.W., Poli, S., 1998. Experimentally based water budgets for dehydrating slabs and consequences for arc magma generation. Earth and Planetary Science Letters 163, 361–379.

Shatsky, V.S., Sobolev, N.V., Stenina, N.G., 1985. Structural peculiarities of pyroxenes from eclogites. Terra Cognita 5, 436–437.

Smith, D.C., 1984. Coesite in clinopyroxene in the Caledonides and its implications for geodynamics. Nature 310, 641–644.

Smith, D.C., 1988. A review of the peculiar mineralogy of the Norwegian coesite–eclogite province, with crystal–chemical, petrological, geochemical and geodynamical notes and an extensive bibliography. In: Smith, D.C. (Ed.), Eclogites and Eclogite-Facies Rocks. Elsevier, Amsterdam.

Sobolev, N.V., Shatsky, V.S., 1990. Diamond inclusions in garnets from metamorphic rocks. Nature 343, 742–746.

Spandler, C.J., Hermann, J., Arculus, R.J., Mavrogenes, J.A., 2003. Redistribution of trace elements during prograde metamorphism from lawsonite blueschist to eclogite facies; implications for deep subduction-zone processes. Contributions to Mineralogy and Petrology 146, 205–222.

Staudigel, H., Plank, T., White, B., Schmincke, H.U., 1996. Geochemical fluxes during seafloor alteration of the basaltic upper oceanic crust: DSDP sites 417 and 418. Subduction Top to Bottom. Geophysical Monograph, vol. 96. American Geophysical Union.

Sun, S.S., McDonough, W.F., 1989. Magmatism in Ocean Basins Chemical and Isotopic Systematics of Ocean Basalts: Implications for Mantle Composition and Processes. Geological Society of London, London.

Tatsumi, Y., Hamilton, D.L., Nesbitt, R.W., 1986. Chemical characteristics of fluid phase released from a subducted lithosphere and origin of arc magmas; evidence from high-pressure experiments and natural rocks. Journal of Volcanology and Geothermal Research 29, 293–309.

Taylor, S.R., McLennan, S.M., 1985. The Continental Crust: Its Composition and Evolution. Blackwell, Oxford.

Taylor, S.R., McLennan, S.M., 1995. The geochemical evolution of the continental crust. Reviews in Geophysics 33, 241–265.

Tsai, C.H., 1998. Petrology and geochemistry of mafic–ultramafic rocks in the North Dabie Complex, central–eastern China. PhD dissertation, Stanford University, Stanford, CA. 171 p.

Tsai, C.H., Liou, J.G., 1997. Inferred ultrahigh-pressure eclogitic metamorphism in the North Dabie Complex, central eastern China. Geological Society of America Abstract With Program 29, A-336.

Tsai, C.H., Liou, J.G., 2000. Eclogite-facies relics and inferred ultrahigh-pressure metamorphism in the North Dabie Complex, central–eastern China. American Mineralogist 85, 1–8.

Tsai, C.H., Liou, J.G., Ernst, W.G., 2000. Petrological characterization and tectonic significance of retrogressed garnet peridotites, Raobazhai area, North Dabie Complex, east-central China. Journal of Metamorphic Geology 18, 181–192.

Wang, X., Liou, J.G., 1991. Regional ultrahigh-pressure coesite-bearing eclogitic terrane in central China: evidence from country rocks, gneiss, marble, and metapelite. Geology 19, 933–936.

Wang, X., Liou, J.G., Mao, H.K., 1989a. Discovery of coesite in the Dabie Mountains, central China; indication of ultra-high pressure metamorphism. Geological Society of America, Annual Meeting, Abstracts with Programs — Geological Society of America, vol. 21.

Wang, X., Liou, J.G., Mao, H.K., 1989b. Coesite-bearing eclogites from the Dabie Mountains in central China. Journal of Geology 17, 1085–1088.

Wilson, M., 1989. Igneous petrogenesis — A global tectonic approach, Unwin Hyman, Oxford University Press, London.

Wilson, S.A., 1997. The collection, preparation, and testing of USGS reference material BCR-2, Columbia River, Basalt. U.S. Geol. Surv. Open-File Report, vol. 98.

Xie, Z., Chen, J., Zhang, X., Gao, T., Dai, S., Zhou, T., Li, H., 2001. Zircon U–Pb dating of gneiss from Shizhube in North Dabie and its geologic implications. Acta Petrologica Sinica 17, 139–144 (in Chinese with English abstract).

Xu, S., Okay, A.I., Sengor, A.M.C., Su, W., Liu, Y., Jiang, L., 1992. Diamond from the Dabie Shan metamorphic rocks and its implication for tectonic setting. Science 256, 80–82.

Xu, S., Liu, Y.C., Jiang, L.L., Su, W., Ji, S.Y., 1994. Tectonic Framework and Evolution of Dabieshan. Science publishing, Beijing (in Chinese with an English extended summary).

Xu, S., Liu, Y., Su, W., Wang, R., Jiang, L., Wu, W., 2000. Discovery of the eclogite and its petrography in the Northern Dabie Mountains. Chinese Science Bulletin 45, 273–278.

Xu, S., Liu, Y., Jiang, L., Wu, W., Chen, G., 2002. Architecture and Kinematics of the Dabie Mountains Orogen. University of Science and Technology of China Press, Hefei.

Yang, J.J., 2003. Titanian clinohumite–garnet–pyroxene rock from the Su–Lu UHP metamorphic terrane, China: chemical evolution and tectonic implications. Lithos 70, 359–379.

Ye, K., Cong, B., Ye, D., 1997. Exsolutions of clinopyroxene, rutile and apatite from garnet in eclogite at Yangkou, Shandong Paninsula, eastern China. Terra Nova 9, 41.

Ye, K., Cong, B., Ye, D., 2000. The possible subduction of continental material to depths greater than 200 km. Nature 407, 734–736.

Zhang, R.Y., Liou, J.G., 1998. Ultrahigh pressure metamorphism of the Sulu terrane Eastern China: a perspective view. Continental Dynamics 3, 32–53.

Zhang, R.Y., Liou, J.G., 1999. Exsolution-lamellae in minerals from ultrahigh-*P* rocks. International Geological Review 41, 981–993.

Zhang, R.Y., Liou, J.G., 2000. Exsolution-lamellae in minerals from ultrahigh-pressure rocks. In: Ernst, W.G., Liou, G.J. (Eds.), Ultrahigh-Pressure Metamorphism and Geodynamics in Collision-Type Orogenic Belts: Geological Society of AmericaInterna-International Book Series, vol. 4, pp. 216–228.

Zhang, R.Y., Liou, J.G., 2003. Clinopyroxenite from Sulu ultrahigh-pressure terrane, eastern China: origin and evolution of garnet exsolution in clinopyroxene. American Mineralogist 88, 1591–1600.

Zhang, R.Y., Liou, J.G., Cong, B.L., 1994. Petrogenesis of garnet-bearing ultramafic rocks and associated eclogites in the Su–Lu ultrahigh-*P* metamorphic terrane, eastern China. Journal of Metamorphic Geology 12, 169–186.

Zhang, R.Y., Liou, J.G., Ernst, W.G., 1995. Ultrahigh pressure metamorphism and decompressional *P–T* path of eclogites and country rocks from Weihai Eastern China. Island Arc 4, 293–309.

Zhang, R.Y., Liou, J.G., Tsai, C.H., 1996. Petrogenesis of a high-temperature metamorphic terrane: a new tectonic interpretation for the north Dabieshan, central China. Journal of Metamorphic Geology 14, 319–333.

Zhang, R.Y., Liou, J.G., Ernst, W.G., Coleman, R.G., Sobolev, N.V., Shatsky, V.S., 1997. Metamorphic evolution of diamond-bearing and associated rocks from the Kokchetav Massif, northern Kazakhstan. Journal of Metamorphic Geology 15, 479–496.

Zhang, R.Y., Zhai, S.M., Fei, Y.W., Liou, J.G., 2003. Titanium solubility in coexisting garnet and clinopyroxene at very high pressure: the significance of exsolved rutile in garnet. Earth and Planetary Science Letters 216, 591–601.